Global and Planetary Change 194 (2020) 103292

Contents lists available at ScienceDirect

Global and Planetary Change

journal homepage: www.elsevier.com/locate/gloplacha

Strain localization during burial and exhumation of the continental upper crust: A case study from the Northern Sporades (Pelagonian thrust sheet, Greece)

Kristóf Porkoláb[a,*], Ernst Willingshofer[a], Dimitrios Sokoutis[a,b], Jan Wijbrans[c]

[a] Department of Earth Sciences, Utrecht University, Utrecht, Netherlands
[b] Department of Geosciences, University of Oslo, Oslo, Norway
[c] Department of Earth Sciences, VU University Amsterdam, Amsterdam, Netherlands

ARTICLE INFO

Keywords:
Strain localization
Mechanical stratigraphy
Structural inheritance
Distributed deformation
Post-orogenic extension
Northern Sporades
Pelagonian

ABSTRACT

Extension is a key process controlling the post-orogenic exhumation of metamorphic rocks in subduction and collision zones. Previous studies have largely focused on the mechanics of localized core-complex style post-orogenic extension and the large-scale effects of various internal (e.g. rheology) and external (e.g. plate motions) parameters on the mode of extension. However, many regions on earth underwent rock exhumation during post-orogenic extension, which is characterized by distributed rather than localized deformation. We explore conditions of distributed deformation as illustrated by the Pelagonian unit in the Aegean subduction system. In particular, we explore the influence of structural inheritance related to the pre-extension shortening and mechanical stratigraphy on the localization of extension on the scale of the upper crust through detailed structural analysis on the islands of Skiathos and Skopelos. Additionally, the time frame of deformation has been established by $^{40}Ar/^{39}Ar$ dating of key shear zones. Shortening on the islands predominantly took place by ductile top-SW thrusting under low-grade metamorphic conditions, localized in weak calcite marble layers within the Upper Cretaceous and Upper Triassic carbonates at ~55 Ma. We show that the presence of shallow decoupling levels in the upper crust resulted in the formation of thin (several 100 m thick) thrust sheets that are defined for the first time on Skiathos. The Early Paleogene accretion of the Pelagonian upper crust to the upper plate (Eurasia/Rhodopia) was followed by the extensional inversion of the nappe stack. Extension was accommodated by opposite-sense, generally top-NE, ductile to brittle shearing, which localized at inherited heterogeneities such as reverse-sense shear zones and stratigraphic contacts at around 35 Ma, as suggested by our $^{40}Ar/^{39}Ar$ age spectra. The dense network of such northerly-dipping, inherited weakness zones resulted in a highly distributed pattern of extensional deformation dominated by layer-parallel shearing. We argue that the distribution of crustal heterogeneities substantially influences the style of post-orogenic extension.

1. Introduction

The burial and exhumation of continental rocks in subduction and collision settings has received significant attention during the last decades. Large-scale analogue and numerical models have demonstrated, that the relative strength (rheology) of the upper crust, lower crust, and lithospheric mantle of continental plates in subduction/collision systems determines where strain localizes and hence controls the geometry of the evolving mountain belt (Sokoutis and Willingshofer, 2011; Vogt et al., 2017; Vogt et al., 2018). In such settings, subduction of continental crust is often followed by post-orogenic extension that is one of the key mechanisms driving the exhumation of deeply buried rocks (e.g. Dewey, 1988; Gautier and Brun, 1994; Lister et al., 1984; Wernicke, 1981). The onset of extensional deformation is often explained by a change in slab dynamics from advancing to retreating (with respect to the upper plate of the subduction system) (Brun and Faccenna, 2008; Brunet et al., 2000; Le Pichon et al., 1981). The distribution of post-orogenic extension is substantially influenced by crustal or lithospheric heterogeneities such as weakness zones inherited from the shortening phase (nappe contacts and suture zones). These weakness zones are prone to be reactivated as extensional faults and shear zones, and may lead to the formation of extensional detachments (e.g. Balázs et al., 2017; Daniel et al., 1996; Jolivet et al., 2010; Patel et al., 1993). Detachments accommodate at least several 10s of

* Corresponding author at: Princetonlaan 4 (Earth Simulation Laboratory), Utrecht, Netherlands.
E-mail address: k.porkolab@uu.nl (K. Porkoláb).

https://doi.org/10.1016/j.gloplacha.2020.103292
Received 27 March 2020; Received in revised form 2 July 2020; Accepted 25 July 2020
Available online 11 August 2020

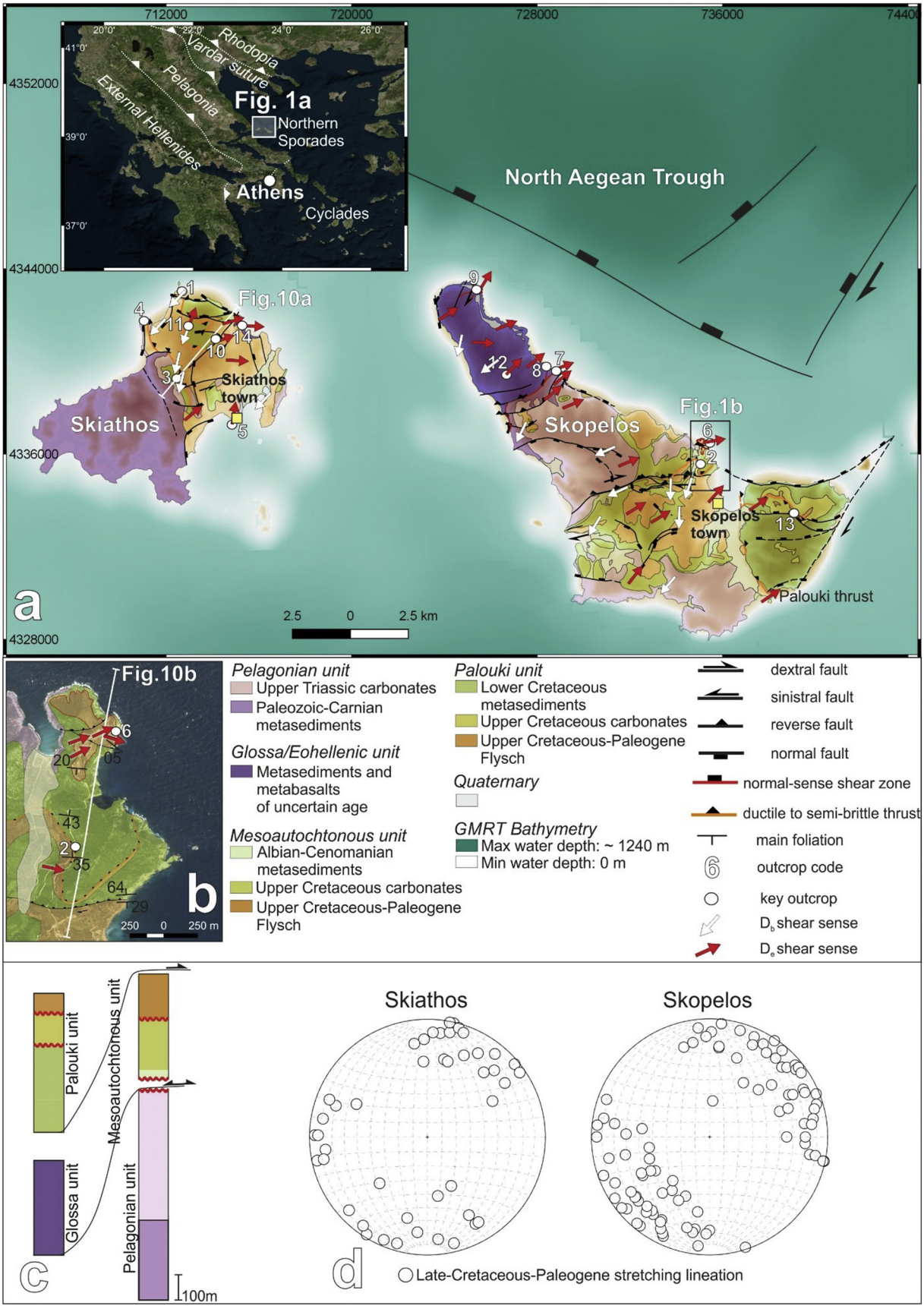

Fig. 1. a) Geological maps of Skiathos (after Ferentinos, 1973) and Skopelos (after Porkoláb et al., 2019) highlighting the locations of key outcrops discussed in the text; b) Magnified detail of Fig. 1a; c) Tectono-stratigraphic column of Skiathos and Skopelos displaying the approximate outcropping thicknesses of the formations and the tectonic units established prior to this study (Ferentinos, 1973; Heinitz and Richter-Heinitz, 1983; Jacobshagen and Wallbrecher, 1984; Matarangas, 1992); d) Stereographic projection of stretching lineations measured on Skiathos and Skopelos.

kilometers of displacement and juxtapose high-grade next to low-grade metamorphic rocks (metamorphic core complexes) (Gautier and Brun, 1994; Reynolds and Spencer, 1985; Wernicke, 1981). The mechanics of detachment faulting and thus the localized mode of post-orogenic extension have been studied extensively (e.g. Axen et al., 1995; Brun et al., 2018; García-Dueñas et al., 1992; Jolivet et al., 2010; Selverstone, 1988), however, less attention have been paid to regions where extensional deformation never resulted in the formation of a major detachment, but is distributed over multiple, smaller shear zones. As a consequence, extensional deformation does not produce easily observable jumps in the metamorphic grade. Furthermore, the relation between the distribution of contractional deformation during nappe stacking and the distribution of subsequent extensional deformation remains unexplored, especially on a smaller, upper crustal scale.

We focus our study on the metasedimentary cover of the Pelagonian thrust sheet (Internal Hellenides) outcropping on the islands of Skiathos and Skopelos (Fig. 1). Different to Rhodopia in the north and the Cyclades in the south, where the extensional style is of localized core-complex type (Brun and Sokoutis, 2007; Brun and Sokoutis, 2018; Gautier and Brun, 1994; Jolivet et al., 2010), extension in our study area is distributed over multiple small-scale (up to a few 10 m thick) extensional shear zones. We aim to understand strain localization on the scale of the Pelagonian metasedimentary cover formations (Late Paleozoic to Paleogene), from the initial stages of shortening, through nappe stacking, to extensional exhumation. We present detailed structural geological analyses supplemented by $^{40}Ar/^{39}Ar$ dating of key shear zones, and discuss the kinematics of burial – exhumation and the importance of mechanical stratigraphy and structural inheritance. We revise the nature of contacts between different geological units on the islands of Skiathos and Skopelos, identifying multiple thrusts and normal-sense shear zones that were previously mapped as stratigraphic contacts (Ferentinos, 1973; Heinitz and Richter-Heinitz, 1983; Matarangas, 1992). We compare our findings on the conditions of distributed extensional shearing with type locations of localized, core-complex-style extension to develop the understanding of post-orogenic extensional strain localization.

2. Tectonic and Geological setting

The Aegean is an excellent location for investigating the burial and exhumation of continental crust, as Cretaceous to Early Paleogene nappe stacking and metamorphism of continental crust was followed by extensional exhumation starting during the Eocene (Brun and Sokoutis, 2007; Hinsbergen and Schmid, 2012; Jolivet and Brun, 2010). This burial-exhumation cycle occurred in context of Africa – Europe convergence, which also led to the closure of the Mesozoic Neotethys ocean and the subduction and accretion of largely upper crustal continental thrust sheets (Pelagonian, Pindos, Gavrovo-Tripolitza, and Ionian thrust sheets) derived from the Adria microplate (Brunn et al., 1976; Jacobshagen, 1978; Jolivet and Brun, 2010; Ricou et al., 1998; Schmid et al., 2019; van Hinsbergen et al., 2005). The accretion of buoyant material to the upper plate (Rhodopia i.e. Eurasia) triggered the retreat of the subduction trench resulting in upper plate extension (Brun and Faccenna, 2008). Following the initiation of slab-rollback, early-stage extension was accommodated by a major top-SW detachment in Rhodopia (Brun and Sokoutis, 2007; Brun and Sokoutis, 2018; Dinter and Royden, 1993; Sokoutis et al., 1993), and a top-NE detachment(s) at the Cyclades (Gautier and Brun, 1994; Jolivet et al., 2010), implying that initial extension was highly localized in those regions. In Neogene times, the rate of slab rollback substantially accelerated following the tearing of the Hellenic slab, resulting in a more distributed pattern of brittle extensional structures related to an increase in mechanical coupling among layers, throughout the Aegean (Brun et al., 2016; Brun, 1999).

The Northern Sporades island group is part of the Pelagonian zone in Greece (Aubouin et al., 1976; Jacobshagen, 1978) and consists of three major islands (Skiathos, Skopelos, and Alonnisos) that are largely made up by low-grade metasediments (Jacobshagen and Wallbrecher, 1984). In the Northern Sporades, the Pelagonian zone consists predominantly of metamorphosed cover sequences and upper crustal rocks that were decoupled from the subducting lower crust and lithospheric mantle during the collision with Eurasia (e.g. Jolivet and Brun, 2010; van Hinsbergen et al., 2005). The oldest outcropping formations are Paleozoic meta-siliciclastics locally intruded by granites, which are overlain by thick (~3 km) Middle Triassic to Middle Jurassic platform carbonates (dolostones and limestone marbles) and a much thinner Middle-Late Jurassic deep water sequence (radiolarites and greywackes). This succession was deposited on the east-facing Pelagonian/Adriatic passive margin (De Bono, 1998; De Bono et al., 2001; Scherreiks, 2000; Scherreiks et al., 2010) and is structurally overlain by obducted Middle-Late Jurassic ophiolites and sub-ophiolitic metasediments that originated in the eastward enclosing Neotethys ocean (Dimo-Lahitte et al., 2001; Scherreiks, 2000; Spray et al., 1984). On the Northern Sporades, the ophiolites that are almost completely eroded (Bortolotti et al., 2013 and references therein; Jacobshagen and Wallbrecher, 1984), and comprise together with the underlying sub-ophiolitic metasediments the Eohellenic nappe (Jacobshagen and Wallbrecher, 1984; Jacobshagen et al., 1978) or the Western-Vardar Ophiolitic unit (Schmid et al., 2019). On Skopelos, the metamafic and metasedimentary rocks of the Eohellenic nappe are referred to as the "Glossa unit", which covers the northern part of the island (Fig. 1a) (Matarangas, 1992). On Skiathos, the Glossa unit was not distinguished on the maps of Ferentinos (1973) or Heinitz and Richter-Heinitz (1983), and it seems to be largely eroded. The Paleozoic-Mesozoic formations below the ophiolites were metamorphosed during the Early Cretaceous, probably related to a phase of continental subduction below the oceanic upper plate (Kilias et al., 2010; Lips et al., 1998; Lips et al., 1999; Most, 2003; Porkoláb et al., 2019). Burial was followed by exhumation, regional erosion, and the deposition of Late Cretaceous-Paleogene sedimentary formations. On the Northern Sporades, the Late Cretaceous – Paleogene formations comprise the Mesoautochtonous unit deposited on Triassic and Jurassic rocks, and the Palouki unit, which was thrust on top of the Mesoautochtonous unit following the deposition of the Upper Cretaceous - Paleogene flysch (Jacobshagen and Wallbrecher, 1984; Matarangas, 1992) (Fig. 1c). These units consist of a transgressive sequence of coarse siliciclastic sediments which are followed by shallow water carbonates (dominantly rudist-bearing limestones), and a quartz-rich flysch succession marking the final closure of the Neotethys ocean (Ferentinos, 1973; Jacobshagen and Wallbrecher, 1984; Matarangas, 1992). On Skiathos, Vidakis (1995) re-interpreted the entire flysch formation as the Eohellenic nappe, however, we consider this erroneous and use the original classification of Ferentinos (1973). During latest Cretaceous – Early Paleogene times, all the formations of the Northern Sporades were affected by tectonic burial leading to greenschist to locally blueschist facies metamorphism, followed by the erosion of the nappe stack and extensional exhumation (Porkoláb et al., 2019). In the following sections we present our results on the strain localization during this phase of burial and exhumation on the islands of Skiathos and Skopelos.

3. Strain localization and the kinematics of deformation

Our fieldwork included detailed mapping of ductile and brittle structures focusing on the kinematics of deformation and delineating the main zones of strain localization. Mapping was based on detailed stratigraphic studies of Skiathos (Ferentinos, 1973; Heinitz and Richter-Heinitz, 1983) and Skopelos (Matarangas, 1992). Regarding the structural build-up of Skopelos, we follow the new map of Porkoláb et al. (2019). We present the results of our structural mapping in the form of geological maps of the two islands (Fig. 1), interpretations of key outcrops (Figs. 2, 3, 4, 5, 6 and 7), and cross sections (Fig. 10).

The pre-Upper Cretaceous formations of the Northern Sporades (the

Paleozoic to Middle Triassic metaclastics and Upper Triassic platform carbonates of the Pelagonian unit, and the Glossa unit) preserve structural elements related to an Early Cretaceous tectono-metamorphic event. In these rocks, the Late-Cretaceous – Paleogene tectono-metamorphic event is already D_2, while in the Upper Cretaceous – Paleogene lithologies it is the first phase, D_1 (Porkoláb et al., 2019). In the present study, we only focus on the Late Cretaceous – Paleogene burial-exhumation cycle which affected all the outcropping formations on Skiathos and Skopelos. Contraction during tectonic burial and extensional exhumation are from now on indexed as D_b and D_e, respectively. Regarding the distribution of deformation in a given rock volume, we use the expressions "localized" and "distributed" always with respect to the scale of observation. Therefore, what is described as "localized" deformation on the scale of the islands, may be part of a "distributed" deformation pattern on a larger scale.

3.1. Contractional structures related to tectonic burial (D_b)

All the geological units of the islands are characterized by a penetrative tectonic foliation (S_b) which is the axial planar cleavage of F_b tight to isoclinal folds. The foliation is poorly or not developed in the dolomitized parts of the Upper Triassic carbonates, but especially well-developed in the calcite marble layers (Figs. 2 and 3). Up to a few hundreds of meters thick calcite marble layers are found in the Upper Triassic part of the Pelagonian unit, and in the Cenomanian – Turonian part of the Mesoautochtonous unit. Thin marble layers are also found in the Glossa unit, which also show well-developed S_b foliation planes (Figs. 6 and 7b). The S_b foliation in the metaclastic rocks (Paleozoic – Carnian part of the Pelagonian unit, some parts of the Glossa unit, and the Upper Cretaceous – Paleogene flysch) is largely defined by recrystallized white micas, chlorite, and occasionally oriented quartz observed macroscopically and in thin sections. The penetrative foliation carries a stretching lineation (L_b) which is defined by stretched calcite aggregates in marbles, and white mica or chlorite in the metaclastic rocks and the metabasalts of the Glossa unit. The best developed stretching lineations are observed in calcite marbles, while stretching lineations in the Upper Cretaceous – Paleogene flysch are often poorly developed. The general trend of stretching lineations is NE-SW on both islands. L_b stretching lineations are generally associated with top-SW to top-S sense of shear described in detail in section 3.1.1., observed on both islands (Fig. 1). These kinematic directions are typically distributed over the entire thickness of the strata. Additionally, localized D_b deformation was also observed in a few, 5–15 m thick shear zones showing a mylonitic foliation, well-developed stretching lineations, and more intense shear fabric compared to the ductile strain recorded outside of these zones. At such shear zones, the Cenomanian – Turonian

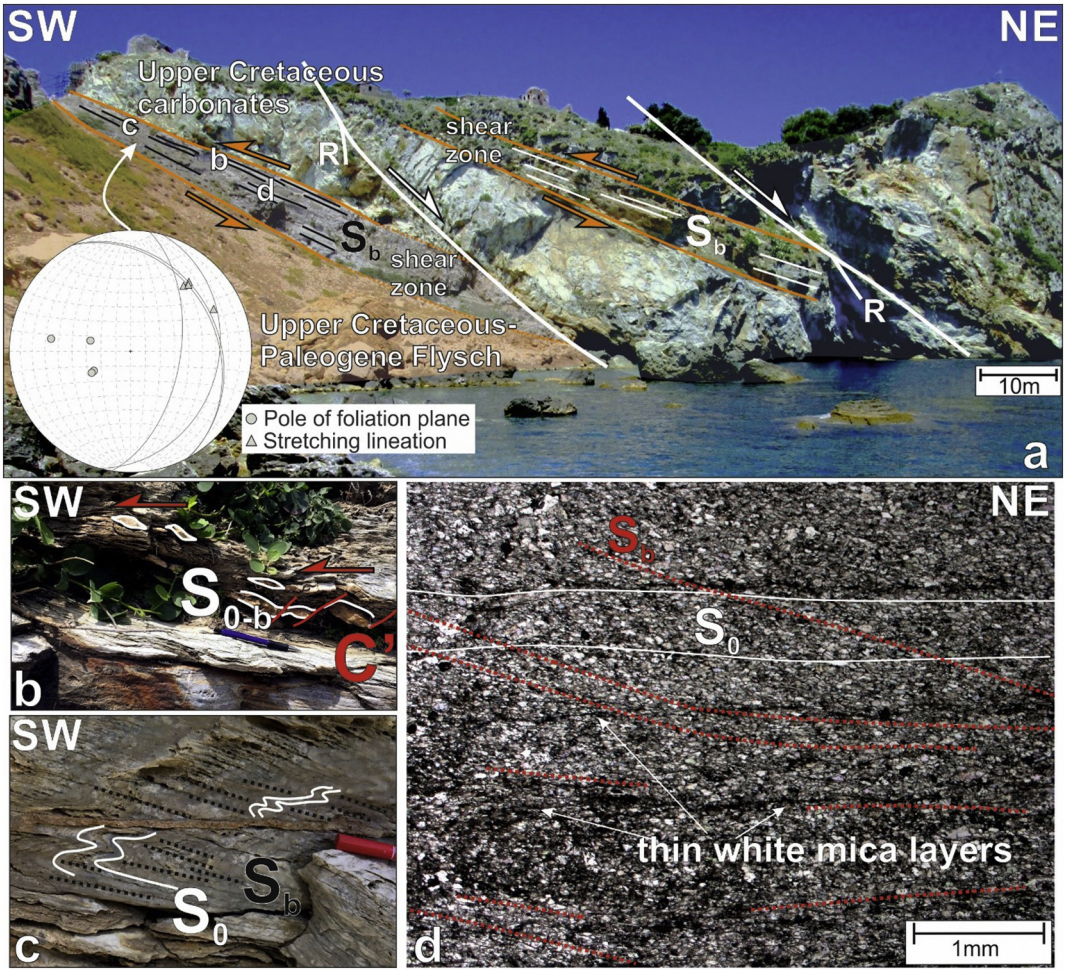

Fig. 2. a) Top-SW reverse-sense shear zone (Kastro shear zone) at Location 1 emplacing the Upper Cretaceous carbonates on top of the Upper Cretaceous-Paleogene Flysch. Stereographic projection of structural measurements is included; b) C′-type shear bands and σ-clasts showing top-SW sense of shear, pencil for scale; c) Relation between the tightly folded S_0 bedding of the marble and the newly formed S_b foliation; d) Plain polarized microscope image of the sample from Location 1 showing the microscale structure of the marble mylonite. Red lines highlight the shape-preferred orientation of the calcite crystals (~95% of the rock mass) that is slightly oblique to the S_0 original bedding (white lines). Discontinuous white mica layers (~5% of the rock mass) follow the S_0 bedding. (For interpretation of the references to colour in this figure legend, the reader is referred to the web version of this article.)

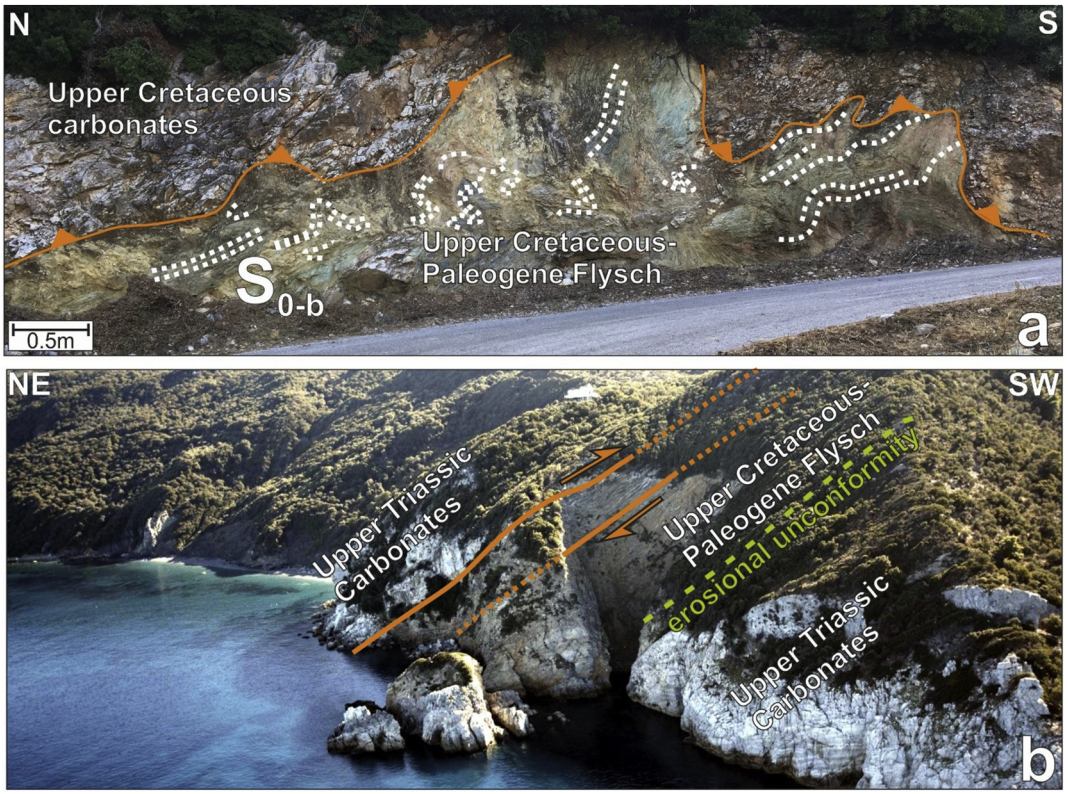

Fig. 3. Key outcrops displaying reverse-sense shear zones. For locations see Fig. 1; a) Folded nappe contact at Location 2 between the Upper Cretaceous carbonates and the Upper Cretaceous-Paleogene Flysch; b) Aerial view (photo from tripinview.com) of a reverse-sense shear zone at Location 4 emplacing the Upper Triassic carbonates on top of the Upper Cretaceous-Paleogene Flysch.

marbles are found on top of the Late Cretaceous – Paleogene flysch unit, or Upper Triassic Pelagonian carbonates on top of the Upper Cretaceous carbonates or flysch of the Mesoautochtonous unit (Fig. 1). Such relationships are observed on both islands at multiple locations, providing the clearest marker for post-Upper Cretaceous thrusting on the Northern Sporades (Figs. 1).

3.1.1. Key outcrops

On Skiathos, the Cenomanian – Santonian carbonates of the Mesoautochtonous unit are in many cases found on top of the younger flysch formation (Fig. 1a). Previous works focusing on lithological mapping defined these as stratigraphic contacts (Ferentinos, 1973; Heinitz and Richter-Heinitz, 1983), not explaining the structural position of the formations.

Location 1 (Kastro shear zone) (Fig. 2a) provides the best exposed section to study this relationship at the historical village of Kastro. The village is built on a cliff made up by the Cenomanian – Santonian carbonates which dip 30–45° to the NE. The flysch (dark grey to brown quartz-rich metasandstones, slates, and phyllites) is outcropping below the carbonates, with an identical orientation. The carbonates show an alternation of well-foliated and massive parts (Fig. 2a), while the flysch carries a moderately developed main foliation (S_b) subparallel with the S_0 compositional layering (bedding), and a weakly developed NE-plunging stretching lineation. The two formations are separated by 5–10 m thick zone with a very closely spaced mylonitic foliation and intense stretching lineations. The mylonitic foliation is NE dipping and carries a down-dip stretching lineation. Both structural elements are similarly oriented as the weakly or moderately developed S_b and L_b in the flysch below, indicating that the tectonic transport along the shear zone was subparallel to the orientation of the S_0 sedimentary foliation. The shear zone consists of nearly pure calcite marble with minor amount (estimated as < 5% based on the thin section) of fine-grained white micas found in discontinuous layers along the S_0 bedding (Fig. 2d). The original bedding is preserved, suggesting that the protolith of the marble mylonite was a well-bedded rather than a massive limestone (Fig. 2a). Shape-preferred orientation of the calcite crystals attesting to dynamic recrystallization defines the S_b foliation that makes a small (10–20°) angle to the S_0 bedding and defines a SW-ward structural vergence (Fig. 2d). This agrees with asymmetric boudinage and σ-clasts showing top-SW sense of shear (Fig. 2b). A similar zone of very well-foliated marble was identified higher up in the outcrop (Fig. 2a). The shear zones are cut by two northerly-dipping normal faults which belong to a later phase of extension. The same top-SW shear zone (Fig. 2a) can be followed from Location 1 towards the South, outcropping at the base of the carbonate hilltops (Fig. 1a).

A similar relationship between the same units is found on the island of Skopelos, at Location 2 (Figs. 1b and 3a). This contact was previously mapped as a stratigraphic contact (Matarangas, 1992), but has recently been identified as a thrust emplacing the carbonates on top of the flysch (Porkoláb et al., 2019). However, the contact and the key structural elements are difficult to analyze and measure, since it has been overprinted by younger deformation phases as shown by the folded, irregular, and brecciated nature of the outcrop (Fig. 3a) and the different structural elements cutting through nearby (Fig. 1b). Both the carbonates and the flysch have a well-developed S_b tectonic foliation, implying that at least one stage of thrusting took place under ductile conditions. To delineate the main structure, detailed mapping of the area was performed, showing that the thrust is dipping in a northerly direction, making a highly curved intersection with the topography (Figs. 1b and 3a). The orientation of the thrust and the S_0—S_b composite foliation in the surrounding outcrops point to a low-angle thrust geometry (Figs. 1b and 3a). The carbonates are characterized by a well-developed tectonic foliation and stretching lineation. However, the L_b stretching lineations that belong to the thrusting have been overprinted by L_e stretching lineations, which locally trend *E*-W and are associated with top-E sense of shear (Fig. 1b). The general orientation of the thrust

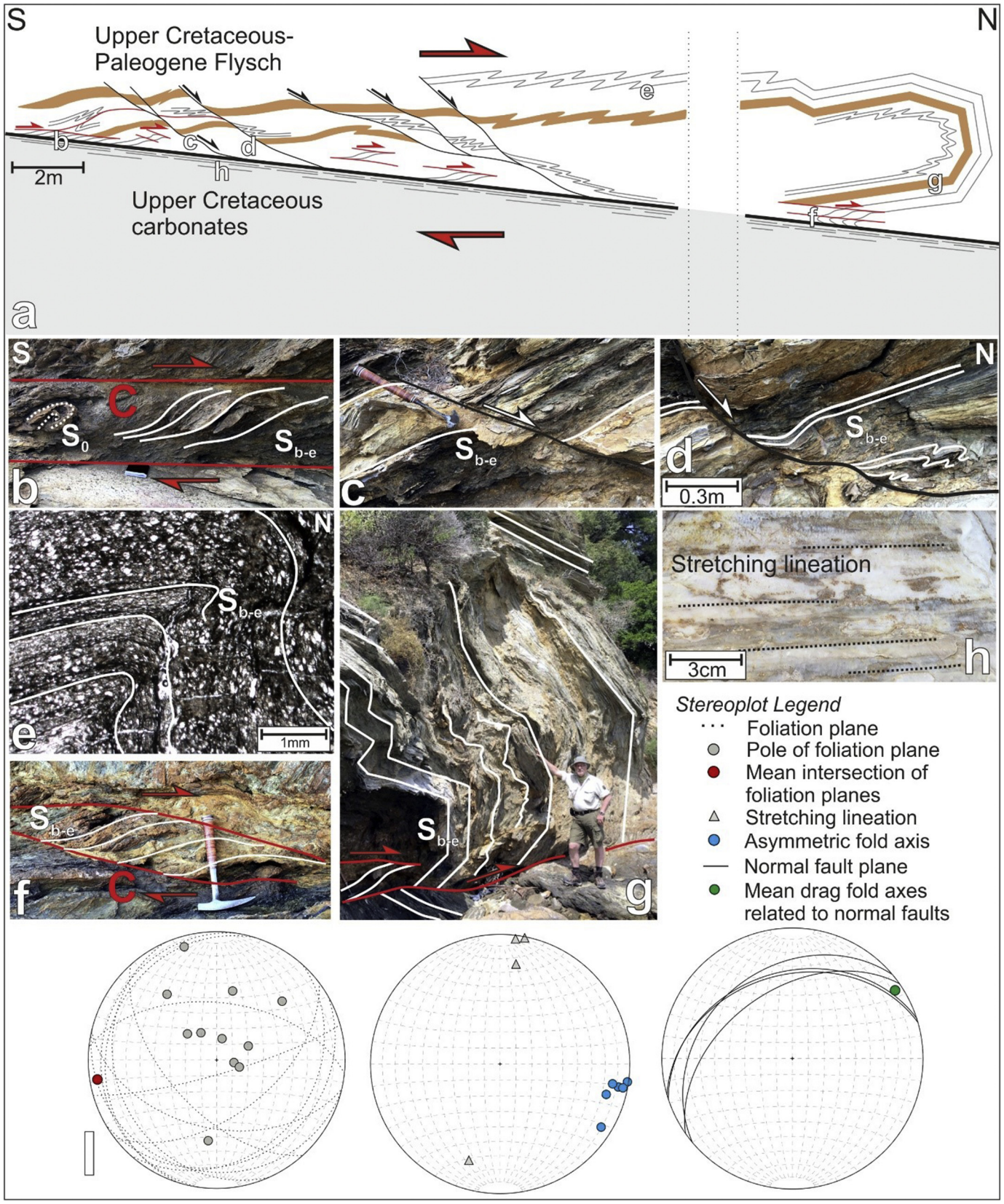

(caption on next page)

and the foliation (N-dipping) in the surrounding rocks, and the frequently observed top-S shearing in the Mesoautochtonous unit on Skopelos (Fig. 1) suggests that the original D_b transport direction at Location 2 was similar to Location 1 on Skiathos, top-S or SW.

Location 3 and 4 on Skiathos exhibit a contact where Upper Triassic carbonates of the Pelagonian unit are lying on top of the Mesoautochtonous unit; in case of Location 3 on the Cenomanian-Santonian carbonates, while in case of Location 4 on the Upper

Fig. 4. a) Top-NNE extensional shear zone at Location 5 activating the stratigraphic contact between the Upper Cretaceous carbonates in the footwall and the Upper Cretaceous-Paleogene Flysch in the hangingwall. Details of the shear zone are highlighted in the subfigures; b) Top-NNE semi-brittle shear bands at the contact of the two formations, notebook for scale; c) NW-dipping, low-angle normal fault, hammer for scale; d) NW-dipping normal fault with semi-brittle asymmetric folds in the hangingwall; e) Plain polarized microscope image of the sample from Location 5 showing a single tectonic foliation that is subparallel to the S_0 bedding. Sedimentary features such as the inverse grading of quartz grains are still visible. The asymmetric top-NNE fold also observed in the outcrop (Fig. 3) did not develop an axial planar cleavage supporting the idea of semi-brittle to brittle flexural folding; f) Ductile top-NNE shear band in the mylonitic contact zone, hammer for scale; g) Recumbent box-fold in the hangingwall of the shear zone, Dimitrios for scale; h) Strong stretching lineation in the footwall marble; i) Stereographic projections of structural elements measured in the outcrop.

Cretaceous-Paleogene flysch (Fig. 1a). At Location 3, Upper Triassic dolomite boulders are found on top of the hill. The dolomites overlie a zone of 5–10 m thick calcite marble with a very closely spaced mylonitic foliation (S_b) that is dipping ~30° to the NE. The mylonitic foliation carries a well-developed N-S trending stretching lineation associated with top-S sense of shear based on asymmetric calcite aggregates and C′ shear bands. The marble mylonites overlie the Upper Cretaceous rudist-bearing carbonates with a less intense $S_{0\text{-}b}$ foliation that has the same, NE-dipping orientation as the mylonites above. The marble mylonites clearly define a shear zone of highly localized strain during top-S ductile thrusting (D_b), similarly to Location 1.

The shear zone is difficult to follow towards the NE due to vegetation and steep topography; however, it crops out on the shoreline cliffs at Location 4 (Figs. 1a and 3b). Here the footwall unit of the ductile thrust is the Upper Cretaceous – Paleogene flysch, which directly overlies the Upper Triassic carbonates with an erosional unconformity (Fig. 3b). The shear zone is delineated by a very well-foliated part below the massive Upper Triassic carbonates in the hangingwall. The white colour of the well-foliated part implies that most of the ductile strain localized in carbonate material similarly to Location 1 or Location 3. The shear zone is subparallel with the main foliation of the outcrop (Fig. 3b).

3.2. Extensional structures related to exhumation (D_e)

Structures that are related to Top-S to SW ductile thrusting and distributed shearing accommodated tectonic burial (D_b) and are often pervasively overprinted by structures related to the extensional exhumation of the rocks from ductile to brittle conditions (D_e). Ductile D_e shearing did in most cases not lead to the formation of a separate S_e foliation. Instead, shearing occurred parallel to the already existing S_b foliation planes, resulting in the deformation of the S_b foliation (Figs. 4, 5, 6, and 7). L_e stretching lineations trend on average NE-SW (Fig. 1) and are defined by the same minerals as L_b such as chlorite, white micas, calcite, and quartz. Therefore, L_b and L_e only differ on the sense of shear, which is generally top-NE in case of D_e and top SW for D_b, respectively (Fig. 1). Top-NE ductile shearing was observed in numerous outcrops on Skopelos and Skiathos (Fig. 1a) and is not restricted to shear zones, attesting to a distributed mode of deformation during D_e phase. Zones of localized D_e strain (i.e. ~ top-NE shear zones) showing a transition from ductile to brittle shearing have been mapped as well and are presented in details in the following section. In zones of localized D_e shear, the meta-basalts of the Glossa unit and occasionally the Upper Cretaceous – Paleogene flysch formation are heavily chloritized (Figs. 7b and c). Strain localization was observed at several inherited reverse-sense shear zones (Figs. 6b and 7a) and stratigraphic contacts (Figs. 4, 5, 6c, and d). D_e shear zones are parallel/subparallel with the $S_{0\text{-}b}$ composite foliation and therefore do not cut out major parts of the stratigraphy. Differences in the metamorphic grade between the footwall and hangingwall of D_e shear zones were also not observed. Ductile top-NE shearing was followed by asymmetric, semi-brittle to brittle, northerly dipping normal faulting observed in many outcrops, providing clear evidence for the extensional nature of top-NE shearing and the gradual change in the deformation conditions from ductile to brittle (Figs. 4, 5, 6, and 7c-e). These northerly dipping normal faults are often tilted and link to pre-existing, ductile to brittle, normal-sense shear zones with similar kinematics (Figs. 4 and 5). Asymmetric (northerly dipping) normal faulting was followed by more symmetric normal faulting (northerly and southerly dipping) as shown by our dataset of mesoscale normal faults measured on both islands (Fig. 8). Two main sets of normal faults can be delineated with no clear overprinting relations between them; one trending NE-SW, and the other trending NW-SE (Fig. 8). The major normal faults (with at least a few tens of meters of displacement, e.g. on Fig. 5a) have been mapped and are presented on Fig. 1, showing that the majority of map-scale normal faults are trending ~ NW-SE (Figs. 1).

3.2.1. Key outcrops

Location 5 (Skiathos town shear zone) at Skiathos city, provides an excellent section to study strain localization during D_e deformation phase. The lower part of the outcrop consists of Upper Cretaceous calcite marbles, which are overlain by the Upper Cretaceous – Paleogene flysch formation (Fig. 4a). The contact is low-angle, on average dipping ~10° to the North. Close to the contact, the marbles exhibit a closely spaced, subhorizontal mylonitic foliation and an intensely developed stretching lineation trending NNE-SSW (Figs. 4h and i). The flysch above is also well-foliated, and consists of quartz-rich, fine-grained metasandstone intercalated with some mica-rich layers. Sericites define the foliation and also the NNE-SSW oriented stretching lineation. Both in the carbonates and the flysch, only one main tectonic foliation is found (S_b—S_e composite foliation) which is subparallel with the original S_0 bedding. The flysch shows an intensely sheared fabric which is best developed close to the contact towards the carbonates. We identified two sets of C-type shear bands; one which rotates the foliation without cutting through the foliation planes, thus attesting to deformation by ductile creep (Fig. 4f), and one which not only drags, but clearly cuts the foliation planes in a brittle manner associated with thin fault gouges or fine-grained breccias along the shear planes (Fig. 4b). Both types of shear bands document the same top-NNE kinematics, providing evidence for perseverant kinematics of the shear zone under decreasing temperature conditions.

The flysch also shows a large number of asymmetric, close to tight folds, which have a consistent top-NNE vergence (Figs. 4a, d, e, and g) and are not developed in the carbonates below. These folds do not have an axial planar cleavage, implying that metamorphic conditions at the stage of folding were probably not high enough to induce ductile creep in the quartz-rich layers (Fig. 4e). Most of these small asymmetric folds are parasitic to a large, recumbent, box-type fold structure which probably formed by flexural slip along the foliation planes of the flysch (Fig. 4g). The folds are cut by numerous small-scale normal faults that have < 1 m displacement (Fig. 1a) and consistently dip towards the NNW (Figs. 4a, c, and d). This represents a continuous record of northward displacement in the shear zone including stages of ductile shearing, semi-brittle shearing and folding, and normal faulting related to extensional exhumation of the rocks. The normal faults are moderately inclined (30–40°) suggesting that the rotation of the shear zone took place during or after its main activity. The shear zone clearly localized at the original stratigraphic contact between the carbonates and the flysch. The carbonates seem to accommodate large amount of ductile strain showing more intense stretching lineation and mylonitic foliation; while semi-brittle and brittle strain is more localized in the metaclastic flysch formation. Fig. 3a shows that the normal faults do

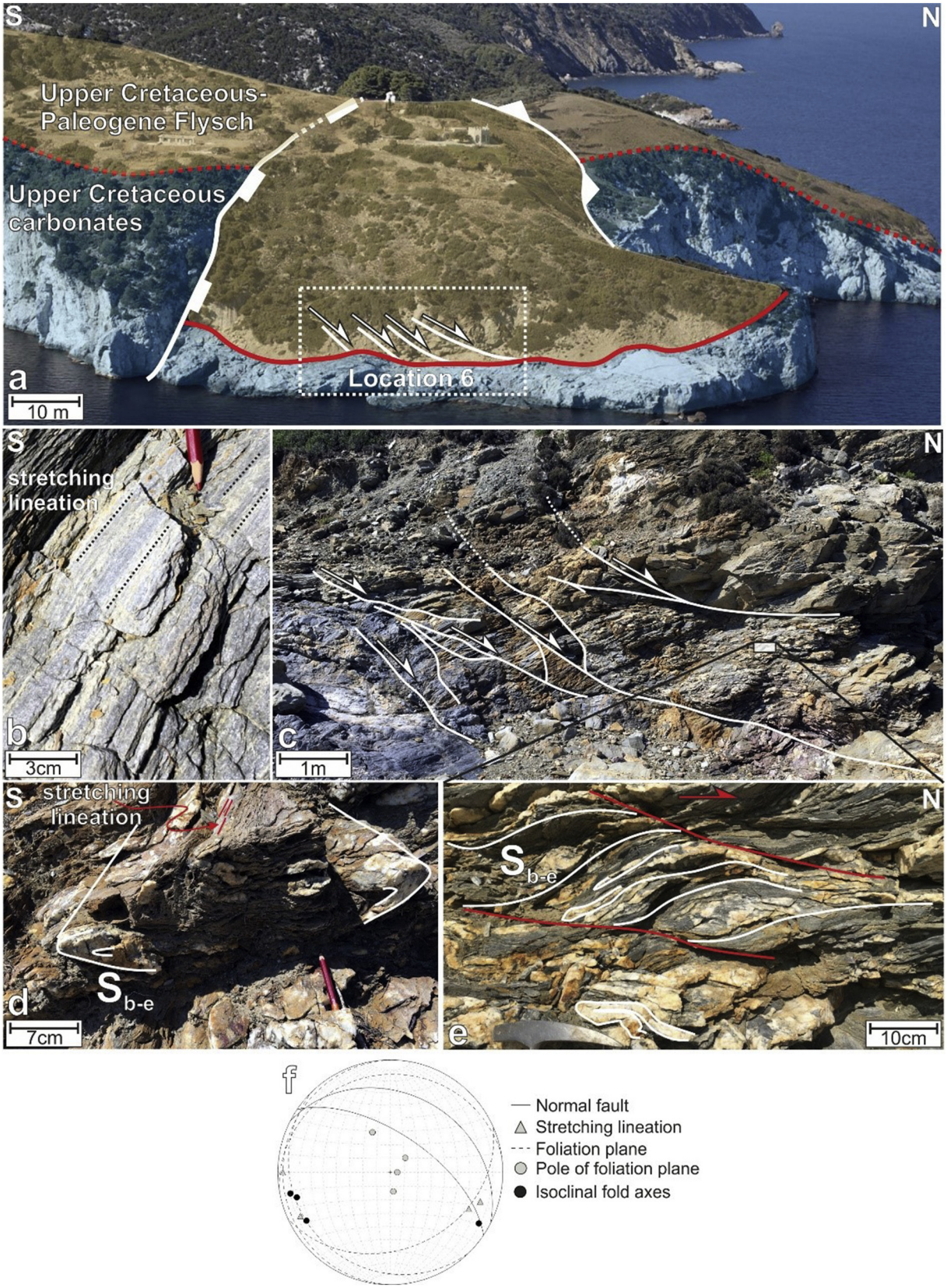

Fig. 5. Top-NE to E extensional shear zone at Location 6 activating the stratigraphic contact between the Upper Cretaceous carbonates and the Upper Cretaceous-Paleogene Flysch. a) Aerial view (photo from tripinview.com) of the shear zone and its surroundings; b) Well-developed stretching lineation; c) A network of flat, NE-dipping normal faults that link to the shear zone below; d) Non-cylindrical (sheath) fold with fold axes subparallel with the stretching lineations; e) Top-NE C–S type shear bands overprinting previously formed isoclinal folds in the shear zone; f) Stereographic projections of structural elements measured in the outcrop.

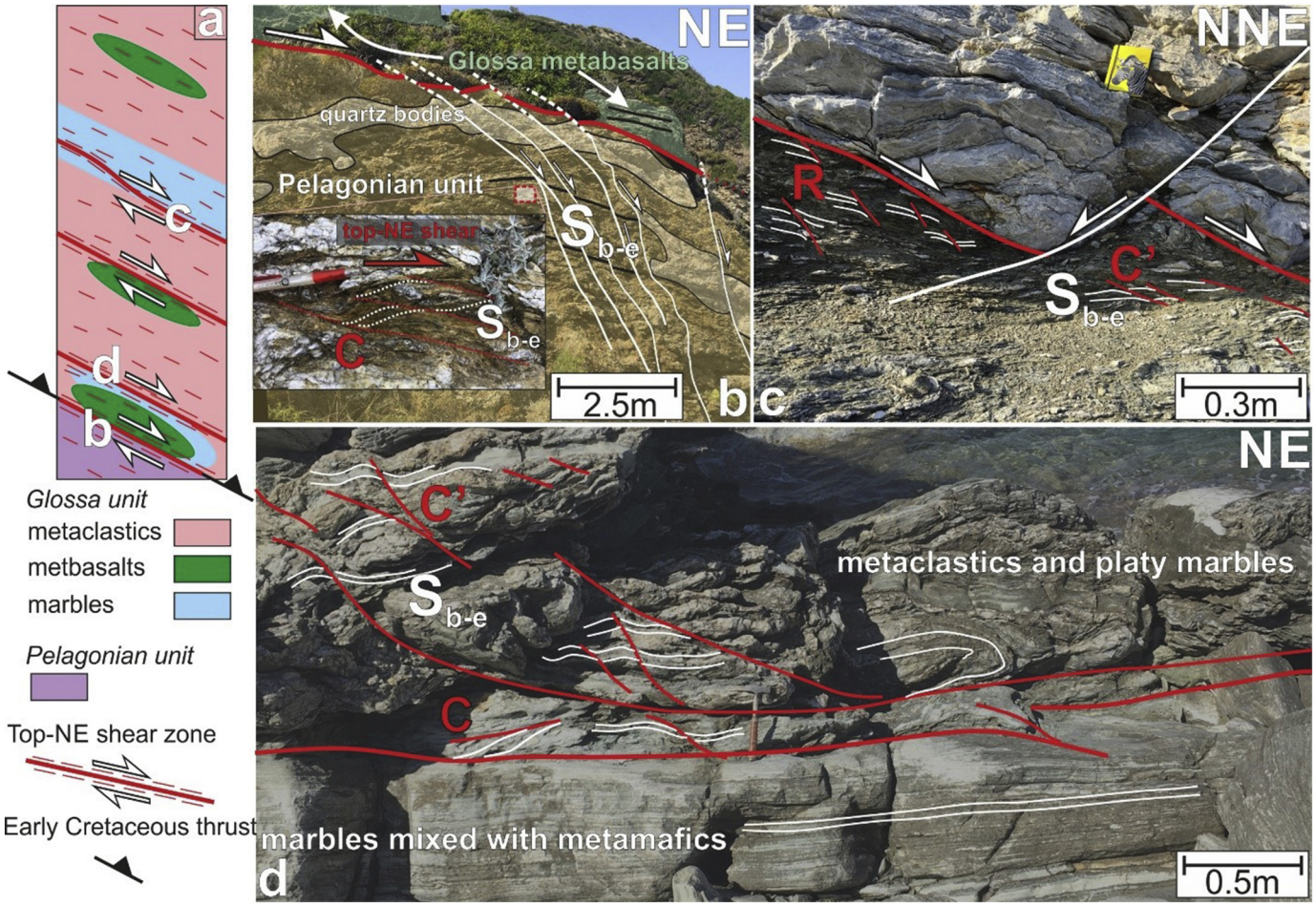

Fig. 6. Extensional strain localization in the Glossa unit, on Skopelos; a) Schematic tectono-stratigraphic column of the Glossa unit, highlighting the position of extensional shear zones and key outcrops; b) Extensional reactivation of the Early Cretaceous nappe contact between the Pelagonian and Glossa units by top-NE shearing and normal faulting, modified after Porkoláb et al. (2019) (Location 7); c) Top-NNE ductile to brittle extensional shear zone between the metaclastic and marble formations of the Glossa unit (Location 9); d) top-NE shear zone between the mixed metabasalt-marble and the metaclastic formations of the Glossa unit (Location 8).

not cut through the contact between the marbles and the flysch, instead they join and reactivate the contact between the two formations which was previously sheared in a ductile manner.

Location 6 on Skopelos (Fig. 5) provides a section that is very similar to Location 5 on Skiathos; it also exhibits Upper Cretaceous carbonates overlain by the Upper Cretaceous – Paleogene flysch formation, with an intensely deformed stratigraphic contact in between (Fig. 5). The Upper Cretaceous marble and the carbonate-rich layers of the flysch show a well-developed mylonitic foliation (S_b—S_e composite foliation) and stretching lineations (Fig. 5b). The stretching lineations trend ESE-WNW to NE-SW (Fig. 5f) and are associated with top-ESE to NE sense of shear evidenced by C-type shear bands (Fig. 5e). Top-ESE to NE shear bands consistently overprint previously formed isoclinal folds (Fig. 5e), but are associated with the formation of non-cylindrical folds (sheath folds) trending subparallel with the stretching lineations (Fig. 5d). The mylonitic foliation and the sheath folds are restricted to the shear zone which is 10–15 m thick. The ductile shear structures have been overprinted by a series of NE-dipping normal faults that joined the main shear zone and reactivated it in a brittle manner (Figs. 5a and c). Some of the normal faults are low-angle, probably attesting to the rotation of the shear zone, while some of them are close to the ideal 60° probably related to a later, post-tilt phase of normal faulting (Fig. 5a). Similarly, to Location 5, this outcrop provides an example for the progressive extensional exhumation of the rocks from ductile shearing to asymmetric normal faulting.

The Glossa unit on Skopelos displays further examples of extensional strain localization (Fig. 6). Fig. 6a shows that the entire Glossa unit was affected by distributed top-NE shearing, while localized top-NE shearing occurred along 1) the inherited Early Cretaceous nappe contact between the Pelagonian and the Glossa units (Fig. 6b, Location 7, discussed in Porkoláb et al. (2019)); 2); the contact between the marbles/metabasalts and the metaclastics (Fig. 6d, Location 8); and 3) the contact between the metaclastic and marble formations (Fig. 6c, Location 9). Location 7 is an outcrop of a 10–15 m thick shear zone separating the Pelagonian and Glossa units, displaying mylonitic foliation, NE-SW trending stretching lineations, top-NE C-type shear bands, and large amount of secondary quartz overgrowth near the main movement zone. The ductile shear zone shows a brittle overprint that does not precisely reactivate the ductile shear zone as a low-angle normal fault, but largely cuts through it with steeper normal faults (Fig. 6b). Location 8 shows a top-NE shear zone between the mixed marbles-metabasalts and the metaclastics of the Glossa unit (Fig. 6d). The calcite-rich footwall rocks have an extremely fine mylonitic foliation and very well-developed NE-SW trending stretching lineations, while the quartz-rich hangingwall shows strong folding and quartz precipitation. Both C and C′-type shear bands were observed, the C′-types showing a transition from ductile (curving the foliation planes) to brittle (cutting the foliation planes) style of deformation. Location 9 displays a ductile to brittle shear zone separating the marbles and metaclastics of the Glossa unit (Fig. 6c). Both rock types were strongly

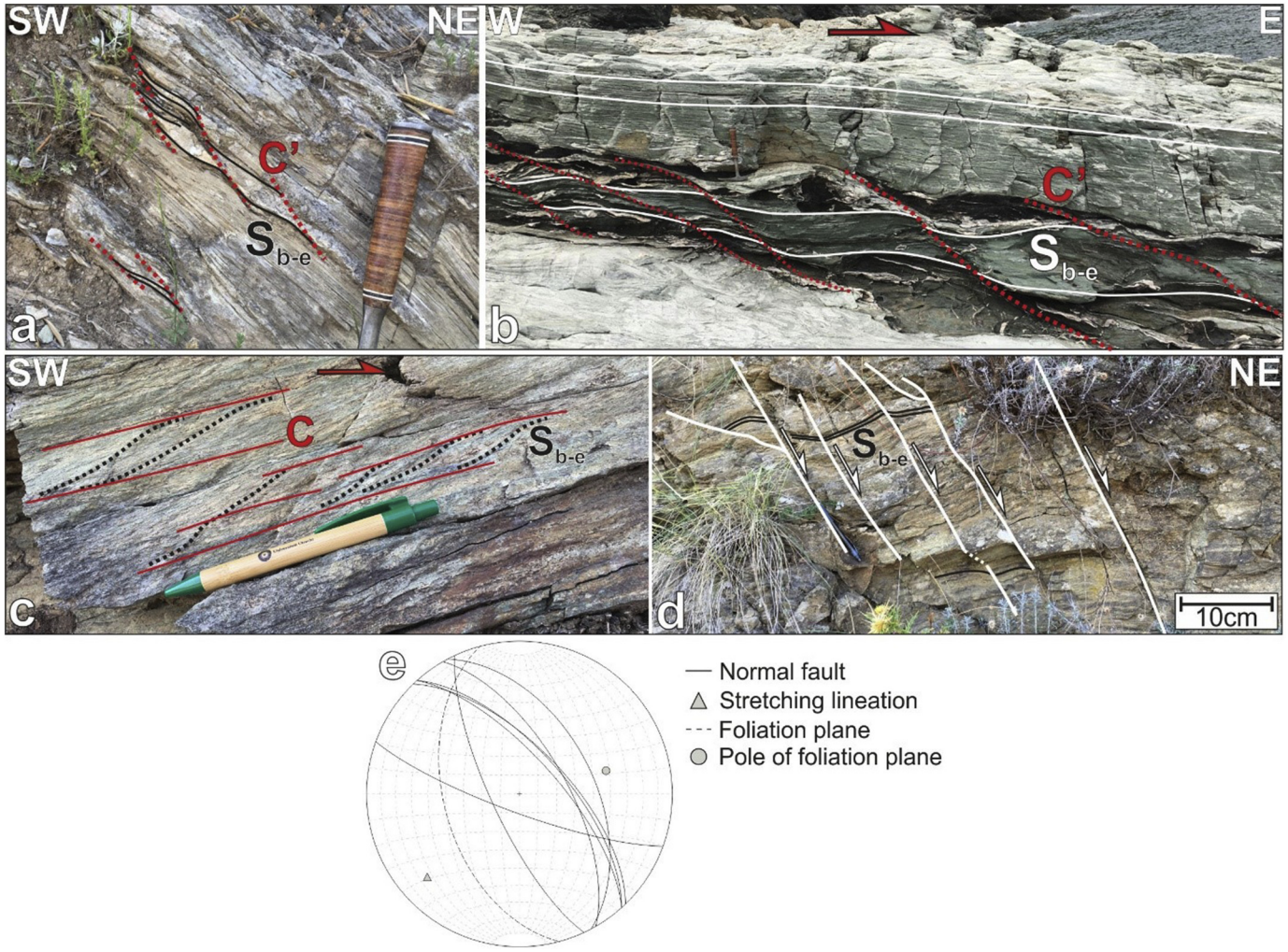

Fig. 7. Examples of top-NE to E extensional shearing; a) Top-NE C′ shear bands at Location 10 showing the reactivation of a top-SW nappe contact that previously emplaced the Upper Cretaceous carbonates on top of the Upper Cretaceous-Paleogene Flysch; b) Well-developed top-E C′ shear bands in the mafic metavolcanics in contact with marbles of the Glossa unit at Location 14. The dark green colour of the metavolcanic rock is related to strong chloritization; c) Top-NE C—S shear bands in the metavolcanics of the Glossa unit at Location 12. The green bands in the rock are heavily chloritized; d) top-NE normal faults in the same outcrop (Location 12) showing to continuity of tectonic transport through the cooling (exhumation) of the rocks; e) Stereographic projections of structural elements measured at Location 12. (For interpretation of the references to colour in this figure legend, the reader is referred to the web version of this article.)

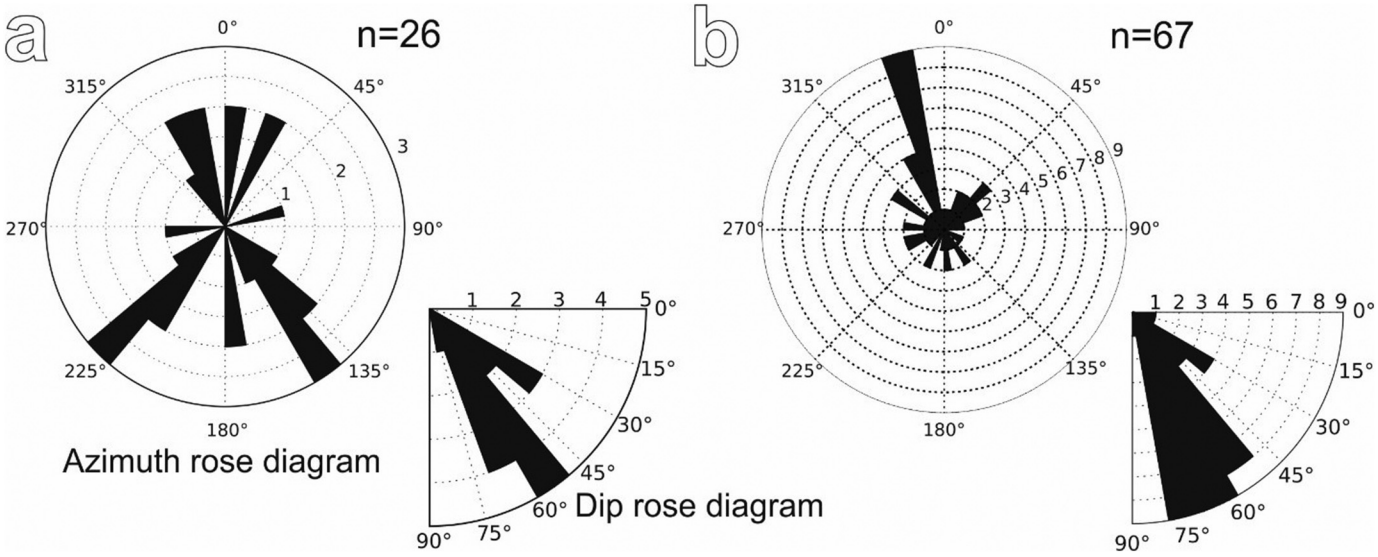

Fig. 8. Azimuth and dip rose diagram of small-scale (up to several meters of displacement) normal faults measured a) on Skiathos; and b) on Skopelos.

sheared and display intense NNE-SSW trending stretching lineations, associated with top-NE C′-type shear bands. The shear zone was reactivated as a brittle, low-angle normal fault as evidenced by cataclastic bands and local brecciaction of the metaclastic rocks. The C′-type ductile shear bands have the same orientation as the overprinting brittle Riedel-planes (Fig. 6b). The foliation planes are cut by the main slip surface at the steeper fault segments, showing that the shear zone was not entirely layer-parallel in the brittle stage.

Locations 10 and 11 on Skiathos are located just above the top-SW ductile thrust that emplaced the Upper Cretaceous carbonates on the of the Upper Cretaceous – Paleogene flysch (Fig. 1a). The outcrops exhibit a shear zone at the base of the marbles with a mylonitic foliation, NE-SW trending stretching lineations, and SW-verging S_0—S_b relations, confirming that we find here the southward continuation of the shear zone at Location 1 (Fig. 2). However, both Locations 10 and 11 show the dominance of opposite, top-NE shear sense indicators within the marble mylonites (Fig. 7a). This implies, that top-NE shearing localized at the pre-existing top-SW shear zone, which was consequently reactivated in an opposite sense.

4. $^{40}Ar/^{39}Ar$ dating of key shear zones

We performed $^{40}Ar/^{39}Ar$ dating of white micas from two key shear zones at Location 1 and Location 5 (Figs. 2 and 4, respectively) in order to constrain the timing of shear zone activity. It has been demonstrated on the island of Skopelos that resetting of the white mica Ar-system in the greenschist facies rocks of the Northern Sporades was achieved by deformation-induced crystallization of the foliation rather than thermally activated diffusion, thus the produced ages can be treated as time constraints for the deformation events (Porkoláb et al., 2019).

In case of Location 1, we sampled the marble mylonites which constitute the shear zone between the Upper Cretaceous carbonates and the Flysch formation below (Fig. 2). The marble consists of > 95% calcite, but contains minor amount of fine-grained white micas (sericite) (Fig. 9a) which were separated in the grain size range of 100–250 μm for the dating, using a Faul vibrating table.

In case of Location 5 (Fig. 4), we sampled the flysch formation which contained sufficient amount of sericite along the foliation planes (Fig. 9b). The individual sericite crystals were too small to be separated, so we used ground mass separates (250–500 μm) following the methodology of Pascual et al. (2013) and Porkoláb et al. (2019).

The samples were packed in aluminium foil packages and stacked in an aluminium tube that was irradiated for 18 h in the CLICIT facility of the Oregon State University TRIGA Reactor. For both irradiations the neutron flux was monitored by standard bracketing with the DRA sanidine standard with an age of 25.52 ± 0.08 Ma, modified from Wijbrans et al. (1995) to be consistent with Kuiper et al. (2008). The step heating experiments were carried out in the Vrije University Amsterdam argon geochronology laboratory with 25 W CO_2 laser heating samples loaded on Cu-trays. The sample holder was connected to a three-stage extraction line and a quadrupole mass spectrometer (Schneider et al., 2009). Data was reduced in ArArCalc 2.50 (Koppers, 2002). Procedure blanks were monitored and diluted air shots were measured in the sequence to track mass discrimination.

4.1. Activity of the Kastro shear zone (Location 1): $^{40}Ar/^{39}Ar$ age spectra

The dated sample from the Kastro shear zone (Location 1) was taken from the marble mylonites that contain ~5% white micas. The thin section displays evidences for deformation by dislocation creep such as sutured grain boundaries, shape preferred orientation, and undulatory extinction (Fig. 9a). The dynamically recrystallized calcite crystals went through grain size reduction during mylonitization as shown by the dominance of ~100 μm grain size and minor amount of remaining larger grains. Fig. 9c shows the age spectra of the white micas separated from the sample. The majority of the heating steps define a dominant ~55 Ma age, while the three early steps show a staircase shape going down to 35–40 Ma (Fig. 9c). Since the resetting of the Ar-system was achieved by deformation-induced crystallization of the white micas during the development of the foliation, we can interpret the ~55 Ma resetting as the main fabric forming event in the shear zone, which was related to the top-SW ductile thrusting. The three-younger steps in the staircase either suggest an overprinting event around 35–40 Ma, or alternatively gradual Ar-loss between ~55 Ma and 35–40 Ma. From a structural geological point of view, continuous deformation and thus foliation development for 20 Myrs is unlikely, therefore we suggest that the 35–40 Ma represents reactivation of the top SW shear zone, which has partially reset the Ar-system of the white micas. This view is in line with our field observations, which show top-NE normal sense reactivation of the shear zone (Fig. 7a).

4.2. Activity of the Skiathos town shear zone: $^{40}Ar/^{39}Ar$ age spectra

Fig. 9d shows the age spectra of the ground mass separates from the Upper-Cretaceous – Paleogene flysch at Location 5 (Skiathos town, Fig. 4). The spectra reveal multiple elements of the history of white micas in the sample. The last heating step yielded an age of ~110 Ma, the previous four steps are in between 55 and 65 Ma, while the last 9 steps define a prominent staircase-shaped spectra ranging from 50 to 30 Ma. The last heating step yielding the oldest age clearly shows that detrital white micas are still present in the flysch, which has also been reported from Skopelos (Porkoláb et al., 2019). The presence of this detrital age confirms that the micas have not been reset by thermal diffusion under greenschist facies conditions, and that not all white micas are reset when the tectonic foliation developed in the rock. The previous four heating steps show ages between 55 and 65 Ma, probably attesting to the same burial-related fabric-forming event that is more dominant in the sample from the Kastro shear zone. This interpretation is supported by microstructural analysis of the dated sample: Fig. 9b shows that our sample preserves inherited structures that were presumably related to burial and associated top-SW shearing and foliation-development, which was not observed in the outcrop (Fig. 4). The 55–65 Ma steps are preceded by 9 steps defining a staircase-pattern, which ranges from ~50 Ma to 30–35 Ma defining a similar young overprinting event as in case of Location 1, yet it seems to be more significant in this sample. The strong overprint is in very good agreement with our observations regarding the top-NNE extensional shearing at Location 5 which gradually shifted to normal faulting (Fig. 4). We suggest that the rocks at Location 5 first developed a tectonic foliation during the top-SW burial of the rocks around 55–60 Ma, which was strongly overprinted by top-NE shearing around 30–35 Ma during the extensional exhumation of the rocks.

5. Discussion

5.1. Implications for the nappe structure of the Northern Sporades

Our field observations led to a substantial revision regarding the tectono-stratigraphy of Skiathos and Skopelos. In case of Skopelos, we use the published map of Porkoláb et al. (2019), but we highlight different structural elements that have not been discussed before, and present a new, smaller scale cross section (Fig. 10b).

In earlier studies, no structures related to post-Cretaceous shortening have been reported from Skiathos. Our field results, maps and cross sections (Figs. 1 and 9), however, show that both Skiathos and Skopelos exhibit several reverse-sense shear zones, which produce repetitions in the upper parts of the stratigraphy. These repetitions were either not observed, or incorrectly interpreted as stratigraphic contacts by previous works on Skiathos (Ferentinos, 1973; Heinitz and Richter-Heinitz, 1983) or Skopelos. On Skiathos, these are 1) the top-SW shear zones outcropping at Locations 1 and 8 that emplaces the Upper Cretaceous carbonates on top of the flysch; and 2) the top-SSW shear zone

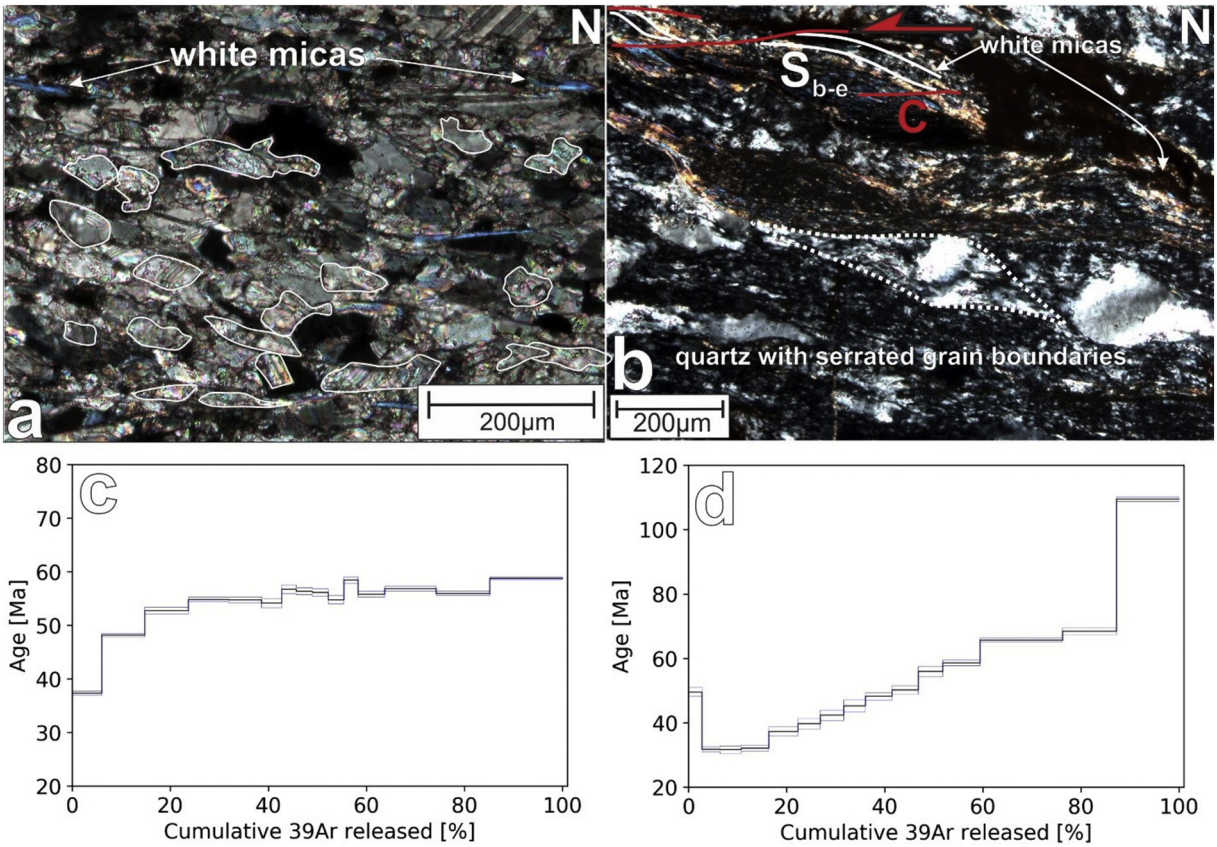

Fig. 9. Results of $^{40}Ar/^{39}Ar$ step heating experiments and microstructural characterization of the dated samples. For locations see Fig. 1; a) Cross polarized image of the sample from Location 1 showing sutured grain boundaries in calcite attesting to deformation by dislocation creep and the presence of white mica flakes that were separated for dating; b) Cross polarized image of the sample from Location 5. The sample largely consists of dynamically recrystallized quartz (~ 90%) and fine-grained white mica crystals. The top-SSW shear criteria presumably attesting to the tectonic burial of the rocks was not observed in the outcrop, which only exhibits top-NNE shear criteria related to extension (Fig. 4); c) Age spectra of the sample from Location 1. d) Age spectra of the sample from Location 5. The horizontal axes show the cumulative ^{39}Ar released during the step heating, while vertical axes show the age of Ar-loss.

outcropping at Location 3 and 4 that emplaces the Upper Triassic carbonates on top of the Upper Cretaceous carbonates or the flysch formation. On Skopelos, these are 1) the N-dipping thrust outcropping at Location 2 that emplaces the Upper Cretaceous carbonates on top of the flysch; and 2) a S-dipping backthrust at Location 10 that similarly emplaces the Upper Cretaceous carbonates on top of the flysch (Figs. 1 and 9).

These structures are all low-angle (< 30°) and produced a tectonic transport that was subparallel with the S_0 bedding in the formations (Fig. 10). Most of the ductile strain was localized in the relatively weak parts of the carbonate formations (Upper Triassic and Upper Cretaceous) that show a well-developed mylonitic foliation and stretching lineation as opposed to the surrounding massive carbonates (partly dolomites, partly massive calcite marbles) and siliciclastic formations. The flat-lying, top-SW shear zones produced small-scale nappes (several 100 m thick) which seem to be rooted in a relatively shallow part of the Pelagonian strata: no hangingwall unit older than Upper Triassic was observed along these thrusts (Fig. 10). The estimated timing of top-SW thrusting on Skiathos (~ 55 Ma in this study) is consistent with the findings of Porkoláb et al. (2019) reporting dominantly 55–65 Ma $^{40}Ar/^{39}Ar$ white mica fabric ages from Skopelos. Our discovery of the D_b shear zones shows that post-Cretaceous shortening was much more pronounced on Skiathos than previously thought (Ferentinos, 1973; Heinitz and Richter-Heinitz, 1983).

5.2. Geometry of upper crustal shortening: The role of stratigraphy

The Aegean consists of exhumed upper crustal thrust sheets derived from the Adria microcontinent, while most of the lower crust and lithospheric mantle subducted into the asthenosphere (Ricou et al., 1998; van Hinsbergen et al., 2005). Decoupling of the upper crust from the rest of the continental lithosphere in numerical models is explained by a major weak zone at the base of the upper crust, defined by the compositional difference between the upper crust and the lower crust (e.g. Vogt et al., 2017). Such models may explain the formation of an upper crustal nappe stack, but lack resolution to account for strain localization in multi-layer systems within the upper crust. In this section, we discuss the intra-upper crustal strain localization during the collision of Pelagonia with Rhodopia based on our key observations.

Our observations suggest that weak calcite layers have played a key role in localizing top-SW shearing following the onset of shortening (Figs. 2 and 3). We have identified two main decoupling levels that determine the geometry of thrusting; namely the relatively weak parts of the Upper Cretaceous and the Upper Triassic shallow-water carbonates (Figs. 2 and 3). In order to understand the stratigraphic control on the thrusting geometries, we discuss the rheology of the initial, pre-shortening (~ 70 Ma) lithological succession of the Pelagonian upper crust (Figs. 11a and b). Our simplified lithological succession consists of (from top to bottom): 1) Upper Cretaceous – Paleogene flysch which is predominantly quartz-rich sandstone; 2) Upper Cretaceous shallow water carbonates containing both massive and layered (weaker) limestones; 3) Ophiolites (mafics and ultramafics) that are partially or completely eroded depending on the exact location, sub-ophiolitic metasediments, siliciclastic sediments of the Albian transgressive sequence; 4) Jurassic and Upper Triassic shallow water carbonates containing both massive, dolomitic, and weaker, layered calcite limestones;

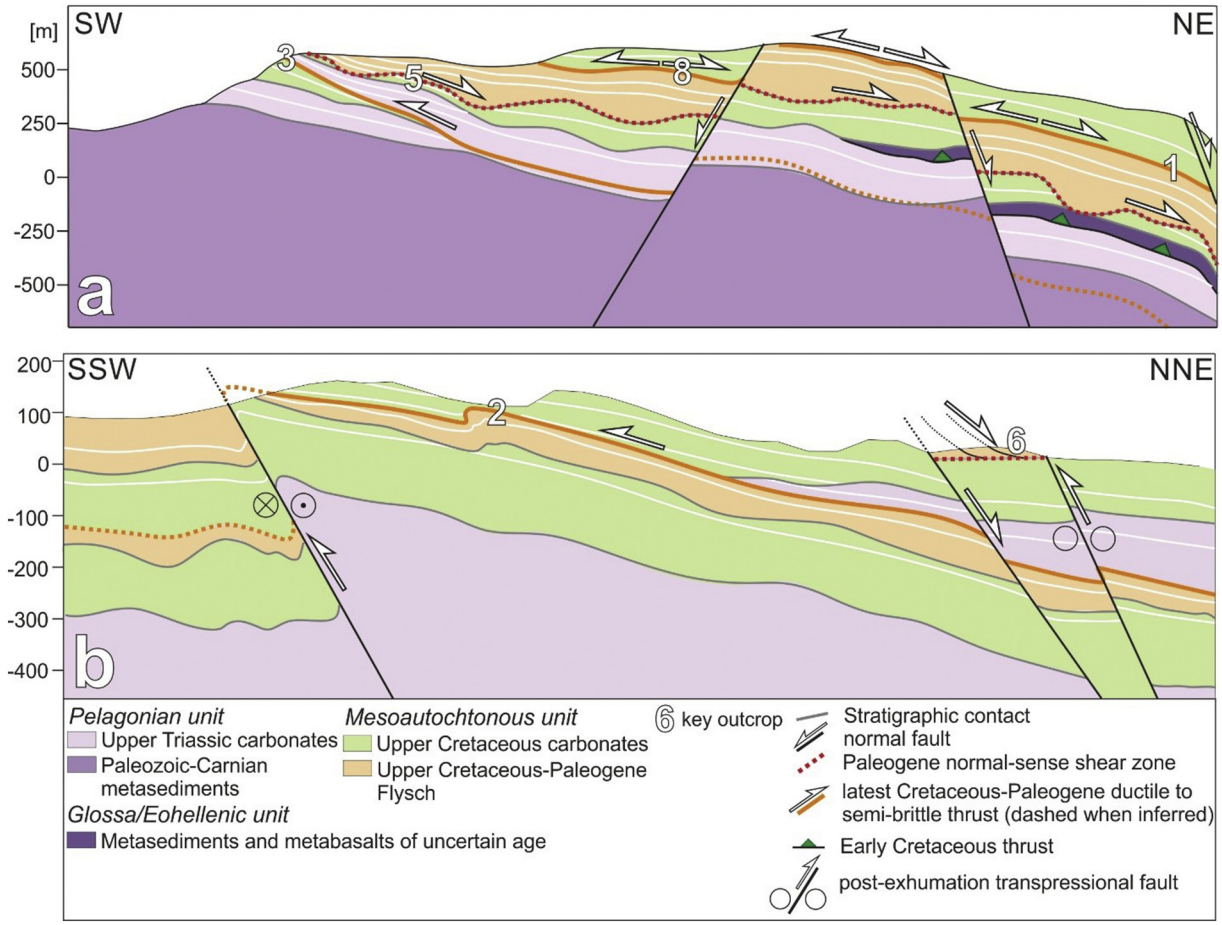

Fig. 10. Cross sections from a) Skiathos; and b) Skopelos. For map-view traces of the cross sections see Fig. 1.

5) Pre-Middle Triassic clastic metasediments and continental crystalline basement rocks.

The observed strain gradients (strain localization in the weak carbonates) suggest that certain parts of the shallow-water carbonates are significantly weaker under low-grade metamorphic conditions than the quartz-rich formations like the Upper Cretaceous – Paleogene flysch. Calcite flow laws based on the assumption that dislocation climb mechanism controls the ductile creep of calcite do not predict such strength differences compared to quartzite flow laws (e.g. Koch et al., 1989; Ranalli, 1995; Schmid et al., 1980). In contrary, a flow law based on the dislocation cross slip mechanism of calcite marbles by De Bresser (2002) predicts creep behavior for calcite layers already at the depth of several kilometers (depending on the geotherm and stress state), resulting in higher predicted strain rates (i.e. strain localization) for calcite layers then for wet quartzites.

We show a simplified strength profile of the top 15 km of the crust considering two calcite layers within the Upper Cretaceous and Upper Triassic carbonate formations which behave according to the cross slip flow law (De Bresser, 2002). All other layers are assumed to behave according to a wet quartzite rheology (Koch et al., 1989) (Fig. 11b). Our calculations show, that the two calcite layers are substantially weaker than the surrounding rocks due to the difference in deformation mechanism (ductile creep for the calcite, brittle failure for the wet quartzite). Consequently, the localization of deformation in the calcite layers is predicted for the shallow upper crust, showing a good fit with our observations (Figs. 2 and 3). Ductile creep in the wet quartzite initiates at the depth of 9–10 km, and around the depth of 13–14 km, the strength of the calcite layers and the wet quartzite become comparable, predicting a more distributed style of deformation. On the scale of the crust, the base of the upper crust (between 15 and 20 km) is still predicted to be the most important weak layer being responsible for the decoupling of the upper crust from the rest of the lithosphere. However, the two weak calcite layers define significant, shallow decoupling horizons, where intra-upper crustal shortening would localize (Fig. 11a and b). The three main ductile shear zones are connected by ductile (below ~10 km) or brittle (above ~10 km) thrust segments, resulting in a ductile flat-brittle ramp type of thrusting geometry (Fig. 11a).

Fig. 11b shows our schematic interpretation of intra-upper crustal thrusting at ~55 Ma. By that time, all the formations reached greenschist facies metamorphic conditions (Porkoláb et al., 2019, this study). Imbrication of the upper crust took place by top-SW thrusting, subparallel to the S_0 bedding in the rocks, coeval to the development of the pervasive S_b tectonic foliation. The presence of two shallow decoupling levels resulted in the formation of thin nappes that are rooted in the upper parts of the original stratigraphy (Fig. 11b).

Our timing constraints with respect to top-SW thrusting and related fabric forming (~ 55 Ma) are consistent with geochronological results from the surrounding regions (Lips et al., 1998; Lips et al., 1999; Most, 2003; Porkoláb et al., 2019; Schermer et al., 1990) and confirm large-scale models that the Pelagonian upper crust accreted to the Eurasian upper plate during early Paleogene times by top-SW thrusting (Brun and Faccenna, 2008; Jolivet and Brun, 2010). Following its accretion, the Pelagonian thrust sheet was emplaced on top of the more external Hellenic units (Fig. 11b and c), namely the Pindos, Gavrovo-Tripolitza, and Ionian upper crustal thrust sheets, which also accreted to the upper plate one-by one, between ~45 and ~ 30 Ma (Jolivet and Brun, 2010; Schmid et al., 2019; van Hinsbergen et al., 2005). The accretion of crustal units to the upper plate triggered the southward retreat of the subduction trench, which has been driving extension in the Aegean

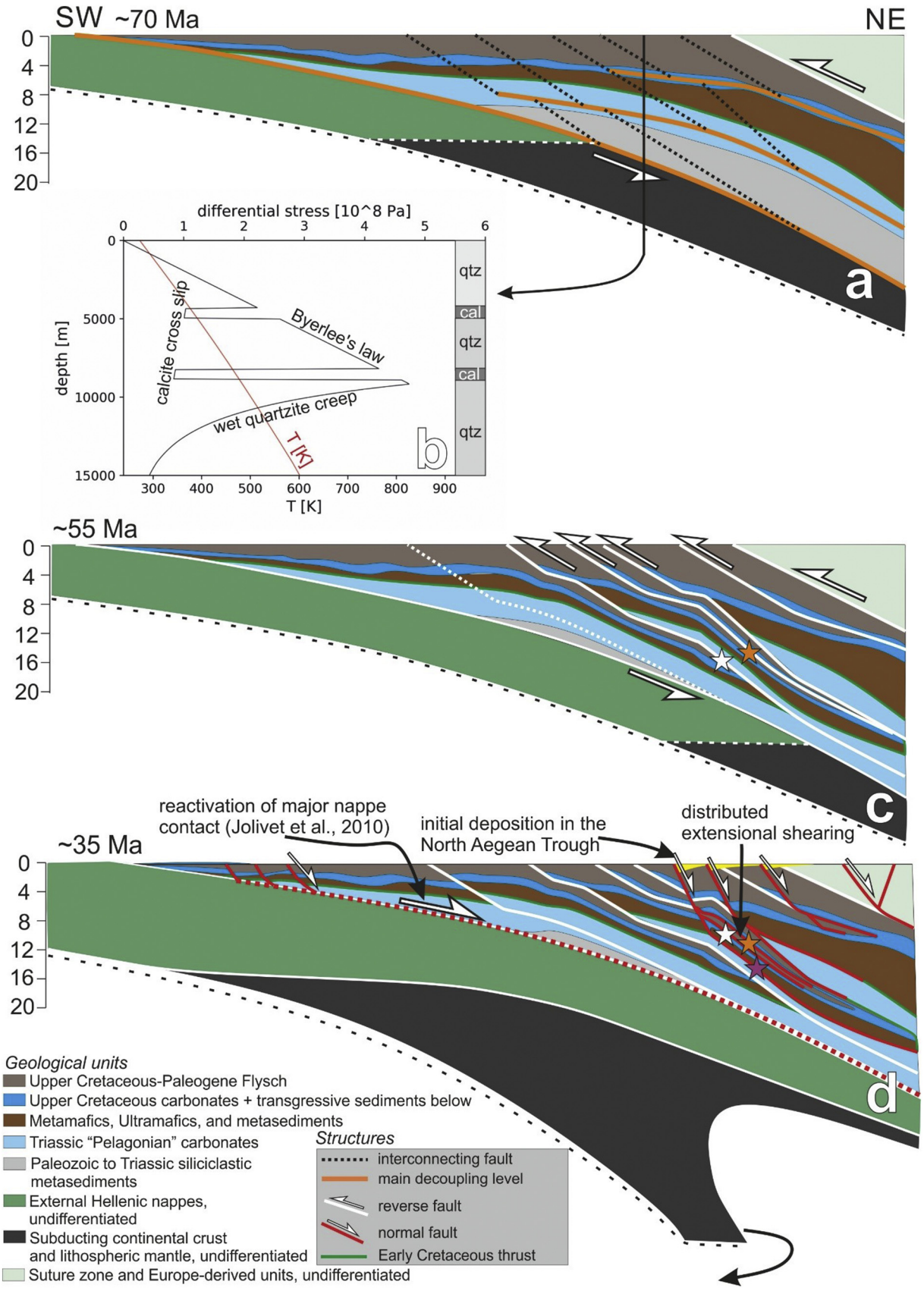

(caption on next page)

Fig. 11. Schematic evolutionary model of the Pelagonian upper crust from ~70 to ~35 Ma; a) Simplified lithological model of the Pelagonian upper crust prior to nappe stacking. The thicknesses of the formations correspond to regional values taken from the literature. The stratigraphic thickness of the flysch formation is difficult to estimate as it is eroded and structurally disrupted to thin slices (e.g. Clift and Robertson, 1989; Sharp and Robertson, 2006; present study), but when it is preserved, it can reach a thickness of a few kilometers (Toljić et al., 2018); b) Strength profile calculated for the uppermost 15 km of the crust assuming an average continental geotherm (corresponding to 65 mW/mˆ2 surface heat flow) and a strain rate of 10ˆ-14 1/s. Two calcite layers are taken into account that follow the calcite cross slip flow law by de De Bresser (2002). The rest of the upper crust is approximated with a wet quartzite rheology (Koch et al., 1989); c) Top-SW nappe stacking at ~55 Ma. The equivalents of our key observations regarding the emplacement of Upper Cretaceous and Upper Triassic carbonates on top of younger formations (Locations 1, 2 and 3, 4) are highlighted by orange and white stars, respectively; d) Top-NE extensional inversion of the nappe stack at ~35 Ma. The equivalents of our key observations regarding the localized shearing at stratigraphic contacts (Figs. 4 and 5), the reactivation of top-SW marble mylonite shear zones (Fig. 7a), and the reactivation of an Early Cretaceous nappe contact are highlighted by orange, white, and purple stars, respectively. (For interpretation of the references to colour in this figure legend, the reader is referred to the web version of this article.)

since ~40 Ma (Bonev et al., 2013; Brun and Sokoutis, 2007; Brun and Faccenna, 2008; Brun et al., 2016; Rohrmeier et al., 2013). The exhumation of the metamorphosed continental nappes is generally attributed to extension, and the role of erosion in the unroofing of the nappe stack is yet to be explored. The proper estimation of the time distribution and the amount of eroded material from the Northern Sporades is presently hindered by the poor quality of available seismic lines and the lack of borehole data in the North Aegean Trough (Beniest et al., 2016).

5.3. Strain localization during extensional exhumation

5.3.1. Geometry and evolution of extensional shear zones

The top-SW nappe stacking was overprinted by opposite sense, on average top-NE, greenschist facies shearing, which we relate to the extension of the Pelagonian nappe stack. The tectonic foliation developed during the burial of the rocks (~ 55 Ma) was deformed and partially recrystallized during extension (~ 30–35 Ma according to the overprinting of the white mica Ar-system). We note that no separate extensional foliation cross-cutting S_b was observed. Most outcrops on both islands display small increments of layer –parallel ~ top-NE shearing (Fig. 7c) implying that the entire thickness of the strata was affected by distributed ductile shearing. Additionally, several sections show localized, ductile to brittle, top-NE shearing on the scale of the islands (Figs. 4, 5, and 6). These extensional shear zones are parallel/subparallel with the pre-existing S_0−S_b foliation, up to 15 m thick, and do not produce an observable difference in the metamorphic grade between the footwall and hangingwall units, attesting to relatively minor displacements (probably up to a few hundreds of meters). Our observations suggest that both stratigraphic and tectonic (thrust) contacts were oriented favorably (dipping to N-NE) to enhance extensional reactivation of these structures (Fig. 11d). Top-SW imbrication developed a dense network of N-NE dipping weak zones (thrust or sheared stratigraphic contacts) which resulted in a characteristic, distributed extensional shearing pattern using multiple small shear zones rather than localization along a single, major detachment (Fig. 11d). These shear zones show evidences of progressive deformation starting under ductile and continuing under brittle conditions (Figs. 4, 5, and 6). We interpret these observations as the gradual extensional exhumation of the rocks starting with top-NE ductile shearing, continuing with transitional shearing, semi-brittle folding, and finishing with normal faulting. Alternatively, the embrittlement of the shear zones due to increasing fluid pressure during mylonitization and mineralization could be envisaged to explain the switch from ductile to brittle shearing (Selverstone et al., 2012). Normal faults that developed in the same rock volume following the localized ductile shearing in the rocks typically appear in asymmetric sets dipping the same way as the shear zones (Figs. 4 and 5). The observation that most of the normal faults join the shear zones rather than crosscutting them (Fig. 4 and 5) suggests that the shear zones remained important decoupling horizons also under brittle conditions and have been reactivated as low-angle normal faults. The majority of the normal faults are rather low-angle (30–40°), implying that rotation took place during the exhumation of the rocks similar to large-scale detachment systems in nature (e.g. Lister and Davis, 1989), or in analogue models (Brun et al., 1994). Alternatively, the formation of low-angle normal faults could be explained by an inclined rather than vertical sigma 1 orientation (Axen, 2019). The key characteristics (relatively small, no linkage with each other, showing transition from ductile to brittle extensional shearing) of the extensional shear zones of Skiathos and Skopelos are identical to the minidetachments described from the proximity of the Whipple detachment in California (Axen, 2019; Axen and Selverstone, 1994). In the case of the Whipple detachment, the linkage of minidetachments at the brittle-ductile transition zone (BDTZ) lead to the formation of the main structure which eventually accommodated most of the displacement (Axen, 2019). Many other detachments over the globe show such strain localization at the BTDZ (e.g. Arca et al., 2010; Martínez-Martínez and Azañón, 1997; Reynolds and Lister, 1990; Selverstone, 1988), and its mechanics has also been shown plausible by numerical and analogue experiments (Brun et al., 1994; Tirel et al., 2008). A key condition for detachment formation at the BDTZ thus is the existence of a favored decoupling level where the normal faults that cut the brittle upper crust are rooted (Fig. 12a). In contrast, Skiathos and Skopelos display multiple decoupling levels defined by the network of N-NE-dipping

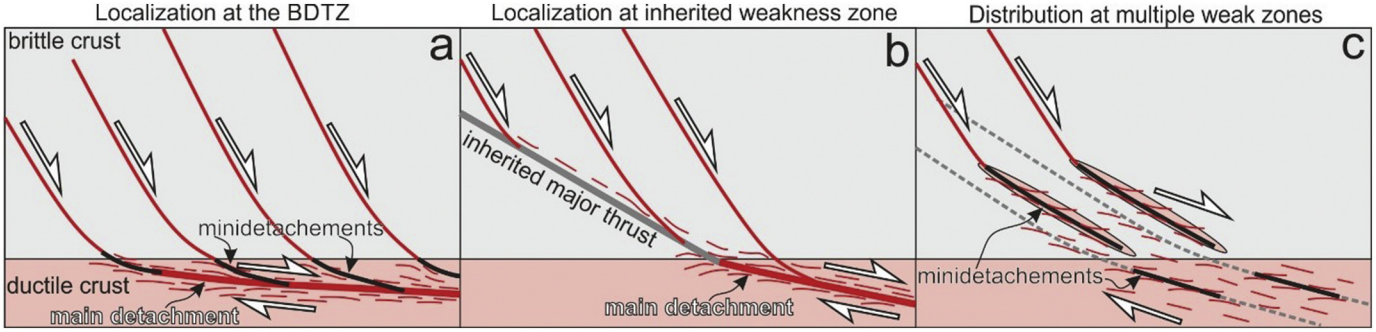

Fig. 12. End-members of extensional strain localization; a) Localization of a detachment at the Brittle-Ductile Transition Zone (BDTZ); b) Localization of a detachment at a major inherited weakness zone (e.g. inherited nappe contact or suture zone); c) Distribution of extensional shearing over multiple weak zones (inherited faults with dashed grey lines), with no major detachment localized due to the lack of linkage between the shear zones.

heterogeneities (Fig. 11d) which resulted in multiple similarly sized (5-15 m thick) shear zones, but no linkages between them. A similar case of distributed extension has been reported from the Apennines, where the W-dipping thrusts of the nappe stack are partially reactivated in extension as low-angle normal faults. These structures do not link up with each other to form a major detachment, and individually accommodate minor amounts of extension (Keller et al., 1994). Fig. 12c shows our simple model of such a distributed style of extension which is accommodated largely by layer-parallel shearing along multiple horizons (minidetachments), and does not result in the formation of a major detachment due to the lack of linkages between the small shear zones. We note however, that the amount of extension applied to the system is certainly crucial. Substantially more extension applied to the nappe stack of the Northern Sporades would most likely have resulted in the linkage of the shear zones to form a major detachment, and a related metamorphic core complex.

5.3.2. The role of structural inheritance in extensional strain localization: The Aegean example

The formation of detachments may also occur by the extensional reactivation of major weakness zones such as nappe contacts; examples have been described from Corsica (Daniel et al., 1996), from the Himalaya (Patel et al., 1993), and from the Aegean (Jolivet et al., 2010). Identically to detachment localization at the BDTZ, the normal faults that cut the upper brittle layer of the crust are rooted in a single detachment which controls the exhumation of the footwall (Figs. 12a and b). Such highly localized extensional patterns have been described from the more external Hellenic thrust sheets outcropping on the northern Cyclades (e.g. Jolivet et al., 2010; Lister et al., 1984) and from Rhodopia (e.g. Brun and Sokoutis, 2007; Sokoutis et al., 1993), standing in contrast with the distributed extensional style of Skiathos and Skopelos.

The Cycladic metamorphic units were exhumed by a top-NE detachment or detachment system, resulting in discrete jumps in the metamorphic grade between footwall and hangingwall units, and the exhumation of higher-grade metamorphic rocks compared to the Northern Sporades. It has been suggested that the localization of the North Cycladic Detachment was controlled by the major top-SW nappe contact separating the formations of the Pelagonian (Internal Hellenic) thrust sheet which did not witness Eocene HP-LT metamorphism from the Pindos/Cycladic blueschist (External Hellenic) units which followed an Eocene HP-LT and Oligocene-Miocene HT-LP metamorphic path (Jolivet et al., 2010 and references therein) (Fig. 11). In contrast, the internal shortening of the Pelagonian thrust sheet - as observed on Skiathos and Skopelos - was characterized by a more distributed thrusting pattern – due to the multiple weak zones in the upper crust - accommodating the shortening on multiple smaller thrusts, hence not producing one prominent rheological weakness zone in the crust. Thus, the difference in the magnitude and localization of post-orogenic, top-NE, extensional shearing between the northern Cyclades and the Northern Sporades may originate in the different distribution of the preceding shortening.

In case of Southern Rhodopia, a highly localized, opposite-sense, top-SW extensional detachment (Kerdylion detachment) controlled the exhumation of a metamorphic core complex consisting largely of amphibolite facies gneisses, marbles, micaschists, and migmatites (Brun and Sokoutis, 2007; Brun and Sokoutis, 2018; Dinter and Royden, 1993; Sokoutis et al., 1993). The reason for the opposite sense of the Kerdylion detachment is yet to be thoroughly investigated, but a possible explanation has been proposed by Jolivet et al. (2018). The authors argue, that back-arc basins opened by slab rollback (such as the Aegean) are subjected to large-scale simple shear induced by the faster trenchward flow of the mantle below the weak crust of the upper plate. The shearing is becoming more effective as the core complexes evolve due to the increasing area affected by the basal drag, and might result in a temporal switch between dominant detachment kinematics; from top-SW (Rhodopia) to top-NE (Cyclades) in case of the Aegean (Jolivet et al., 2018). In addition to this, we suggest, that the opposite sense of the Kerdylion detachment might also be influenced by structural inheritance. In contrast with the Adria-derived tectonic units, Rhodopia was subjected to a change in subduction polarity, from SW-dipping during the Jurassic and Early Cretaceous to NE-dipping during the Late Cretaceous – Paleogene (e.g. Jahn-Awe et al., 2010). The former SW-dipping subduction resulted in the formation of major top-NE thrusts which produced a penetrative SW-dipping fabric in the rocks (Bonev and Stampfli, 2003; Okay et al., 2001; Schmid et al., 2019). These structures might have controlled strain localization during the Eocene extension and localized the main detachment along a SW-dipping pre-existing weak zone.

5.4. Late-stage brittle extension

The initial geometry of the normal faulting linked to the flat-lying decoupling horizons was characterized by asymmetric, predominantly northerly-dipping fault sets which often have been rotated (Figs. 4, 5, and 10d). However, following the further exhumation of the rocks, more symmetric (both northerly and southerly dipping) normal faults formed, most of which have not been substantially rotated based on their dip angle (Fig. 8), and accommodated map-scale extensional deformation (Figs. 1 and 9). Widespread normal faulting and related development of Neogene basins in the Aegean has been attributed to the acceleration of slab-rollback from ~15 Ma, possibly induced by the tearing of the Hellenic slab (Brun and Sokoutis, 2010; Brun et al., 2016). We suggest that the majority of non-tilted, symmetric normal fault sets on Skiathos and Skopelos are related to this accelerated phase of extension during the Neogene. This idea is supported by the thick (possibly up to 6 km) Neogene sediments deposited in the North Aegean trough north of Skopelos (Beniest et al., 2016; Jongsma, 1975; Mascle and Martin, 1990) (Fig. 1). The small-scale faults (up to a several meters of displacements) have a highly varying orientation with no clear evidence for overprinting relations between the differently oriented sets, thus making a paleostress analysis of the faults pointless (Fig. 8). The two main sets (NW-SE trending and NE-SW trending) of small-scale normal faults imply perpendicular extensional directions, corresponding to trench-perpendicular (~NE-SW) and trench-parallel (~NW-SW) directions in reference to the Hellenic subduction zone. It has been suggested that trench-perpendicular extension driven by trench retreat and trench-parallel extension driven by the opposite-sense rotation of the eastern and western Aegean are of comparable magnitude (Hinsbergen and Schmid, 2012). Trench-parallel extension resulted in the enhanced thinning of the South Aegean nappe stack, however, its effect must have been much less in the North Aegean where oroclinal bending was not as pronounced (Hinsbergen and Schmid, 2012). Our maps and cross sections show that the majority of the map-scale faults (minimum a few tens of meters of displacement) are oriented roughly NW-SE on Skiathos and Skopelos, supporting the idea that trench-perpendicular extension has been predominant in the area of the Northern Sporades (Figs. 1 and 9). However, the presence of numerous NE-SW trending small-scale faults (Fig. 8) suggests that the second and third principal stress axes (σ_2 and σ_3) had roughly the same magnitude for a period of time, allowing the switch from NE-SW to NW-SE oriented σ_3.

6. Concluding remarks

We presented a case study on how strain is distributed within a major upper crustal nappe (Pelagonian thrust sheet), from the initial stages of tectonic burial to the extensional exhumation of the formations. Detailed structural analysis on two islands (Skiathos and Skopelos) supplemented by $^{40}Ar/^{39}Ar$ dating of key shear zones led to the following conclusions:

- The Northern Sporades display several thin thrust sheets consisting

of shallow upper crustal formations. Our structural mapping resulted in the definition of two thrust contacts on Skiathos that are reported here for the first time.

- Thrusting predominantly took place by ductile top-SW shearing under low-grade metamorphic conditions, localized in weak calcite marble layers within the Upper Cretaceous and Upper Triassic carbonates at ~55 Ma. We show that the rheological heterogeneity defined by the pre-shortening stratigraphy is key in understanding strain localization during the tectonic burial of the continental upper crust. The multiple decoupling levels in the upper crust of the Northern Sporades resulted in distributed top-SW thrusting, i.e. the formation of thin, small-scale nappes.
- Our kinematic and timing constraints support model implications suggesting that extension initiated following the Early Paleogene accretion of the Pelagonian upper crust to Eurasia (e.g. Brun and Faccenna, 2008).
- Extensional inversion of the nappe stack initiated by opposite-sense, generally top-NE, ductile shearing, which localized at inherited heterogeneities such as reverse-sense shear zones and stratigraphic contacts at ~35 Ma. The dense network of northerly-dipping, inherited weakness zones resulted in a highly distributed pattern of ductile extensional deformation (layer-parallel shearing). The shear zones did not link up with each other and consequently no major extensional detachment formed. We argue that the contrasting distribution and kinematics of post-orogenic extension in the different regions of the Aegean (Cyclades, Northern Sporades, and Southern Rhodopia) was influenced by structural inheritance.
- Ductile top-NE shearing was gradually replaced by semi-brittle shearing and normal faulting attesting to the extensional exhumation of the rocks. Dominantly northerly dipping normal faulting linked to the northerly dipping decoupling levels was later replaced by more symmetric normal faulting. The orientation of normal faults suggests variable extensional directions (mainly trench-perpendicular and trench-parallel), with the predominance of NE-SW, trench-perpendicular extension.

Declaration of Competing Interest

The authors declare no conflict of interests.

Acknowledgements

This publication is dedicated to the memory of Ferenc (Frank) Horváth. We thank Prof. Dr. Hans de Bresser and Prof. Dr. Gary Axen for their important insights on the rheological behavior of calcite and on the mechanics of detachment formation, respectively. We further thank the reviewers for their constructive feedback. The research leading to these results has received funding from the European Union's MSCA-ITN-ETN Project SUBITOP 674899.

References

Arca, M.S., Kapp, P., Johnson, R.A., 2010. Cenozoic crustal extension in southeastern Arizona and implications for models of core-complex development. Tectonophysics 488 (1–4), 174–190.

Aubouin, J., Bonneau, M., Davidson, J., Leboulenger, P., Matesco, S., Zambetakis, A., 1976. Esquisse structurale de l9Arc egeen externe; des Dinarides aux Taurides. Bulletin de la Societé géologique de France 7 (2), 327–336.

Axen, G.J., 2019. How a strong low-angle normal fault formed: the Whipple detachment, southeastern California. Geol. Soc. Am. Bull. https://doi.org/10.1130/B35386.1.

Axen, G.J., Selverstone, J., 1994. Stress state and fluid-pressure level along the Whipple detachment fault, California. Geology 22 (9), 835–838.

Axen, G.J., Bartley, J.M., Selverstone, J., 1995. Structural expression of a rolling hinge in the footwall of the Brenner Line normal fault, eastern Alps. Tectonics 14 (6), 1380–1392.

Balázs, A., Burov, E., Matenco, L., Vogt, K., Francois, T., Cloetingh, S., 2017. Symmetry during the syn-and post-rift evolution of extensional back-arc basins: the role of inherited orogenic structures. Earth Planet. Sci. Lett. 462, 86–98.

Beniest, A., Brun, J.-P., Gorini, C., Crombez, V., Deschamps, R., Hamon, Y., Smit, J., 2016. Interaction between trench retreat and Anatolian escape as recorded by Neogene basins in the northern Aegean Sea. Mar. Pet. Geol. 77, 30–42.

Bonev, N., Spikings, R., Moritz, R., Marchev, P., Collings, D., 2013. 40Ar/39Ar age constraints on the timing of Tertiary crustal extension and its temporal relation to ore-forming and magmatic processes in the Eastern Rhodope Massif, Bulgaria. Lithos 180, 264–278.

Bonev, N.G., Stampfli, G.M., 2003. New structural and petrologic data on Mesozoic schists in the Rhodope (Bulgaria): geodynamic implications. Compt. Rendus Geosci. 335 (8), 691–699.

Bortolotti, V., Chiari, M., Marroni, M., Pandolfi, L., Principi, G., Saccani, E., 2013. Geodynamic evolution of ophiolites from Albania and Greece (Dinaric-Hellenic belt): one, two, or more oceanic basins? Int. J. Earth Sci. 102 (3), 783–811.

Brun, J.P., 1999. Narrow rifts versus wide rifts: inferences for the mechanics of rifting from laboratory experiments. *Philosophical Transactions of the Royal Society of London.* Series A: Mathematical, Physical and Engineering Sciences 357 (1753), 695–712.

Brun, J.-P., Faccenna, C., 2008. Exhumation of high-pressure rocks driven by slab rollback. Earth Planet. Sci. Lett. 272 (1), 1–7.

Brun, J.P., Sokoutis, D., 2018. Core complex segmentation in North Aegean, a dynamic view. Tectonics 37 (6), 1797–1830.

Brun, J.-P., Sokoutis, D., 2007. Kinematics of the southern Rhodope core complex (North Greece). Int. J. Earth Sci. 96 (6), 1079–1099.

Brun, J.-P., Sokoutis, D., 2010. 45 my of Aegean crust and mantle flow driven by trench retreat. Geology 38 (9), 815–818.

Brun, J.-P., Sokoutis, D., Van Den Driessche, J., 1994. Analogue modeling of detachment fault systems and core complexes. Geology 22 (4), 319–322.

Brun, J.-P., Faccenna, C., Gueydan, F., Sokoutis, D., Philippon, M., Kydonakis, K., Gorini, C., 2016. The two-stage Aegean extension, from localized to distributed, a result of slab rollback acceleration 1. Can. J. Earth Sci. 53 (11), 1142–1157.

Brun, J.-P., Sokoutis, D., Tirel, C., Gueydan, F., Van den Driessche, J., Beslier, M.-O., 2018. Crustal versus mantle core complexes. Tectonophysics 746, 22–45.

Brunet, C., Monié, P., Jolivet, L., Cadet, J.-P., 2000. Migration of compression and extension in the Tyrrhenian Sea, insights from 40Ar/39Ar ages on micas along a transect from Corsica to Tuscany. Tectonophysics 321 (1), 127–155.

Brunn, J., Argyriadis, I., Ricou, L., Poisson, A., Marcoux, J., De Graciansky, P., 1976. Eléments majeurs de liaison entre Taurides et Hellénides. Bulletin de la Societé géologique de France 7 (2), 481–497.

Clift, P.D., Robertson, A.H., 1989. Evidence of a late Mesozoic Ocean basin and subduction-accretion in the southern Greek Neo-Tethys. Geology 17 (6), 559–563.

Daniel, J.-M., Jolivet, L., Goffe, B., Poinssot, C., 1996. Crustal-scale strain partitioning: footwall deformation below the Alpine Oligo-Miocene detachment of Corsica. J. Struct. Geol. 18 (1), 41–59.

De Bono, A., 1998. Pelagonian Margins in Central Evia Island (Greece): Stratigraphy and Geodynamic Evolution. Université de Lausanne.

De Bono, A., Martini, R., Zaninetti, L., Hirsch, F., Stampfli, G.M., Vavassis, I., 2001. Permo-Triassic stratigraphy of the pelagonian zone in central Evia island (Greece). Eclogae Geol. Helv. 94, 289–311.

De Bresser, J. (2002), On the mechanism of dislocation creep of calcite at high temperature: Inferences from experimentally measured pressure sensitivity and strain rate sensitivity of flow stress. *J. Geophys. Res. Solid Earth*, *107*(B12), ECV 4–1-ECV 4–16.

Dewey, J., 1988. Extensional collapse of orogens. Tectonics 7 (6), 1123–1139.

Dimo-Lahitte, A., Monié, P., Vergély, P., 2001. Metamorphic soles from the Albanian ophiolites: Petrology, 40Ar/39Ar geochronology, and geodynamic evolution. Tectonics 20 (1), 78–96.

Dinter, D.A., Royden, L., 1993. Late Cenozoic extension in northeastern Greece: Strymon Valley detachment system and Rhodope metamorphic core complex. Geology 21 (1), 45–48.

Ferentinos, G.C., 1973. The geology-petrology of the island of Skiathos. Δελτίον της Ελληνικής Γεωλογικής Εταιρίας 10 (2), 323–358.

García-Dueñas, V., Balanyá, J., Martínez-Martínez, J., 1992. Miocene extensional detachments in the outcropping basement of the northern Alboran basin (Betics) and their tectonic implications. Geo-Mar. Lett. 12 (2–3), 88–95.

Gautier, P., Brun, J.-P., 1994. Crustal-scale geometry and kinematics of late-orogenic extension in the Central Aegean (Cyclades and Ewia Island). Tectonophysics 238 (1–4), 399–424.

Heinitz, W., Richter-Heinitz, I., 1983. Geologische Unteersuchungen im Nordost-Teil der Insel Skiathos (Griechenland). Berliner geowissenschaftliche Abhandlungen,(A) *48*, 41–63.

Hinsbergen, D.J., Schmid, S.M., 2012. Map view restoration of Aegean–West Anatolian accretion and extension since the Eocene. Tectonics 31 (5).

van Hinsbergen, D.J.J., Hafkenscheid, E., Spakman, W., Meulenkamp, J., Wortel, R., 2005. Nappe stacking resulting from subduction of oceanic and continental lithosphere below Greece. Geology 33 (4), 325–328.

Jacobshagen, V., 1978. Structure and Geodynamic Evolution of the Aegean Region.

Jacobshagen, V., Wallbrecher, E., 1984. Pre-Neogene nappe structure and metamorphism of the North Sporades and the southern Pelion peninsula. Geol. Soc. Lond., Spec. Publ. 17 (1), 591–602.

Jacobshagen, V., Skala, W., Wallbrecher, E., 1978. Alpine structure and development of the southern Pelion peninsula and the North Sporades. Alps, Apennines, Hellenides Sci Report 38, 484–488.

Jahn-Awe, S., Froitzheim, N., Nagel, T.J., Frei, D., Georgiev, N., Pleuger, J., 2010. Structural and geochronological evidence for Paleogene thrusting in the western Rhodopes, SW Bulgaria: elements for a new tectonic model of the Rhodope Metamorphic Province. Tectonics 29 (3).

Jolivet, L., Brun, J.-P., 2010. Cenozoic geodynamic evolution of the Aegean. Int. J. Earth Sci. 99 (1), 109–138.

Jolivet, L., Lecomte, E., Huet, B., Denèle, Y., Lacombe, O., Labrousse, L., Le Pourhiet, L., Mehl, C., 2010. The north cycladic detachment system. Earth Planet. Sci. Lett. 289 (1–2), 87–104.
Jolivet, L., Menant, A., Clerc, C., Sternai, P., Bellahsen, N., Leroy, S., Pik, R., Stab, M., Faccenna, C., Gorini, C., 2018. Extensional crustal tectonics and crust-mantle coupling, a view from the geological record. Earth Sci. Rev. 185, 1187–1209.
Jongsma, D., 1975. A Marine Geophysical Study of the Hellenic Arc. University of Cambridge.
Keller, J., Minelli, G., Pialli, G., 1994. Anatomy of late orogenic extension: the Northern Apennines case. Tectonophysics 238 (1–4), 275–294.
Kilias, A., Frisch, W., Avgerinas, A., Dunkl, I., Falalakis, G., Gawlick, H.J., 2010. Alpine architecture and kinematics of deformation of the northern Pelagonian nappe pile in the Hellenides.
Koch, P.S., Christie, J.M., Ord, A., George Jr., R.P., 1989. Effect of water on the rheology of experimentally deformed quartzite. J. Geophys. Res. Solid Earth 94 (B10), 13975–13996.
Koppers, A.A., 2002. ArArCALC—software for 40 Ar/39 Ar age calculations. Comput. Geosci. 28 (5), 605–619.
Kuiper, K., Deino, A., Hilgen, F., Krijgsman, W., Renne, P., Wijbrans, J.R., 2008. Synchronizing rock clocks of Earth history. Science *320* (5875), 500–504.
Le Pichon, X., Angelier, J., Osmaston, M., Stegena, L., 1981. The Aegean Sea [and Discussion]. Philosophical Transactions of the Royal Society of London A: Mathematical, Physical and Engineering Sciences 300 (1454), 357–372.
Lips, A., White, S., Wijbrans, J., 1998. 40 Ar/39 Ar laserprobe direct dating of discrete deformational events: a continuous record of early Alpine tectonics in the Pelagonian Zone, NW Aegean area, Greece. Tectonophysics 298 (1), 133–153.
Lips, A., Wijbrans, J., White, S., 1999. New insights from 40Ar/39Ar laserprobe dating of white mica fabrics from the Pelion Massif, Pelagonian Zone, Internal Hellenides, Greece: implications for the timing of metamorphic episodes and tectonic events in the Aegean region. Geol. Soc. Lond., Spec. Publ. 156 (1), 457–474.
Lister, G.S., Davis, G.A., 1989. The origin of metamorphic core complexes and detachment faults formed during Tertiary continental extension in the northern Colorado River region. USA. 11, 65–94.
Lister, G.S., Banga, G., Feenstra, A., 1984. Metamorphic core complexes of Cordilleran type in the Cyclades, Aegean Sea, Greece. Geology 12 (4), 221–225.
Martínez-Martínez, J., Azañón, J., 1997. Mode of extensional tectonics in the southeastern Betics (SE Spain): Implications for the tectonic evolution of the peri-Alborán orogenic system. Tectonics 16 (2), 205–225.
Mascle, J., Martin, L., 1990. Shallow structure and recent evolution of the Aegean Sea: a synthesis based on continuous reflection profiles. Mar. Geol. 94 (4), 271–299.
Matarangas, D., 1992. Geological Investigation of Skopelos Island. North Sporades, *Greece*, Forschungszentrum Jülich, Zentralbibliothek.
Most, T., 2003. Geodynamic evolution of the Eastern Pelagonian Zone in northwestern Greece and the Republic of Macedonia. *Implications from U/Pb, Rb/Sr, K/Ar, Ar/Ar, geochronology and fission track thermochronology. Tubingen, Phd.* Germany 1-170.
Okay, A., Satır, M., Tüysüz, O., Akyüz, S., Chen, F., 2001. The tectonics of the Strandja Massif: late-Variscan and mid-Mesozoic deformation and metamorphism in the northern Aegean. Int. J. Earth Sci. 90 (2), 217–233.
Pascual, F.J.R., Arenas, R., Catalán, J.R.M., Fernández, L.R.R., Wijbrans, J.R., 2013. Thickening and exhumation of the Variscan roots in the Iberian Central System: Tectonothermal processes and 40Ar/39Ar ages. Tectonophysics 587, 207–221.
Patel, R., Singh, S., Asokan, A., Manickavasagam, R., Jain, A., 1993. Extensional tectonics in the Himalayan orogen, Zanskar, NW India. Geol. Soc. Lond., Spec. Publ. 74 (1), 445–459.
Porkoláb, K., Willingshofer, E., Sokoutis, D., Creton, I., Kostopoulos, D., Wijbrans, J., 2019. Cretaceous-Paleogene tectonics of the Pelagonian zone: inferences from Skopelos island (Greece). Tectonics. 38, 1946–1973.
Ranalli, G., 1995. Rheology of the Earth. Springer Science & Business Media.
Reynolds, S.J., Lister, G.S., 1990. Folding of mylonitic zones in Cordilleran metamorphic core complexes: evidence from near the mylonitic front. Geology 18 (3), 216–219.
Reynolds, S.J., Spencer, J.E., 1985. Evidence for large-scale transport on the Bullard detachment fault, west-Central Arizona. Geology 13 (5), 353–356.
Ricou, L.-E., Burg, J.-P., Godfriaux, I., Ivanov, Z., 1998. Rhodope and Vardar: the metamorphic and the olistostromic paired belts related to the cretaceous subduction under Europe. Geodin. Acta 11 (6), 285–309.
Rohrmeier, M.K., Von Quadt, A., Driesner, T., Heinrich, C.A., Handler, R., Ovtcharova, M., Ivanov, Z., Petrov, P., Sarov, S., Peytcheva, I., 2013. Post-orogenic extension and hydrothermal ore formation: High-precision geochronology of the central rhodopian metamorphic core complex (Bulgaria-Greece). Econ. Geol. 108 (4), 691–718.
Schermer, E.R., Lux, D.R., Burchfiel, B.C., 1990. Temperature-time history of subducted continental crust, Mount Olympos Region, Greece. Tectonics 9 (5), 1165–1195.
Scherreiks, R., 2000. Platform margin and oceanic sedimentation in a divergent and convergent plate setting (Jurassic, Pelagonian Zone, NE Evvoia, Greece). Int. J. Earth Sci. 89 (1), 90–107.
Scherreiks, R., Bosence, D., BouDagher-Fadel, M., Meléndez, G., Baumgartner, P.O., 2010. Evolution of the Pelagonian carbonate platform complex and the adjacent oceanic realm in response to plate tectonic forcing (late Triassic and Jurassic), Evvoia, Greece. Int. J. Earth Sci. 99 (6), 1317–1334.
Schmid, S.M., Paterson, M.S., Boland, J.N., 1980. High temperature flow and dynamic recrystallization in Carrara marble. Tectonophysics 65 (3–4), 245–280.
Schmid, S.M., Fügenschuh, B., Kounov, A., Matenco, L., Nievergelt, P., Oberhänsli, R., Pleuger, J., Schefer, S., Schuster, R., Tomljenović, B., 2019. Tectonic units of the Alpine collision zone between Eastern Alps and Western Turkey. Gondwana Res. 78, 308–374.
Schneider, B., Kuiper, K., Postma, O., Wijbrans, J., 2009. 40Ar/39Ar geochronology using a quadrupole mass spectrometer. Quat. Geochronol. 4 (6), 508–516.
Selverstone, J., 1988. Evidence for east-west crustal extension in the Eastern Alps: Implications for the unroofing history of the Tauern Window. Tectonics 7 (1), 87–105.
Selverstone, J., Axen, G.J., Luther, A., 2012. Fault localization controlled by fluid infiltration into mylonites: Formation and strength of low-angle normal faults in the midcrustal brittle-plastic transition. J. Geophys. Res. Solid Earth 117 (B6).
Sharp, I.R., Robertson, A.H., 2006. Tectonic-sedimentary evolution of the western margin of the Mesozoic Vardar Ocean: evidence from the Pelagonian and Almopias zones, northern Greece. Geol. Soc. Lond., Spec. Publ. 260 (1), 373–412.
Sokoutis, D., Willingshofer, E., 2011. Decoupling during continental collision and intraplate deformation. Earth Planet. Sci. Lett. 305 (3–4), 435–444.
Sokoutis, D., Brun, J., Van Den Driessche, J., Pavlides, S., 1993. A major Oligo-Miocene detachment in southern Rhodope controlling North Aegean extension. J. Geol. Soc. 150 (2), 243–246.
Spray, J., Bébien, J., Rex, D., Roddick, J., 1984. Age constraints on the igneous and metamorphic evolution of the Hellenic-Dinaric ophiolites. Geol. Soc. Lond., Spec. Publ. 17 (1), 619–627.
Tirel, C., Brun, J.P., Burov, E., 2008. Dynamics and structural development of metamorphic core complexes. J. Geophys. Res. Solid Earth 113 (B4).
Toljić, M., Matenco, L., Stojadinović, U., Willingshofer, E., Ljubović-Obradović, D., 2018. Understanding fossil fore-arc basins: Inferences from the cretaceous Adria-Europe convergence in the NE Dinarides. Glob. Planet. Chang. 171, 167–184.
Vidakis, M., 1995. Geological map of Greece 1, 50.000.
Vogt, K., Matenco, L., Cloetingh, S., 2017. Crustal mechanics control the geometry of mountain belts. Insights from numerical modelling. Earth Planet. Sci. Lett. 460, 12–21.
Vogt, K., Willingshofer, E., Matenco, L., Sokoutis, D., Gerya, T., Cloetingh, S., 2018. The role of lateral strength contrasts in orogenesis: a 2D numerical study. Tectonophysics 746, 549–561.
Wernicke, B., 1981. Low-angle normal faults in the Basin and Range Province: nappe tectonics in an extending orogen. Nature 291 (5817), 645.
Wijbrans, J., Pringle, M., Koppers, A., Scheveers, R., 1995. Argon geochronology of small samples using the Vulkaan argon laserprobe, paper presented at Proceedings of the Royal Netherlands Academy of Arts and Sciences.